JOURNAL OF SPACECRAFT AND ROCKETS
Vol. 56, No. 3, May–June 2019

GRACE-FO: The Gravity Recovery and Climate Experiment Follow-On Mission

Richard P. Kornfeld,* Bradford W. Arnold,† Michael A. Gross,‡ Neil T. Dahya,§
and William M. Klipstein¶
Jet Propulsion Laboratory, California Institute of Technology, Pasadena, California 91109
Peter F. Gath**
Airbus Defence and Space GmbH, 88090 Immenstaad, Germany
and
Srinivas Bettadpur††
University of Texas at Austin, Austin, Texas 78759

DOI: 10.2514/1.A34326

The Gravity Recovery and Climate Experiment Follow-On mission was conceived to continue the successful legacy of the recently decommissioned Gravity Recovery and Climate Experiment mission and, at the same time, serve as a platform to demonstrate the first-ever in-space intersatellite laser ranging interferometer as a technology pathfinder for future gravity mapping missions. Launched in May of 2018, the Gravity Recovery and Climate Experiment Follow-On observatory builds on the design of the original Gravity Recovery and Climate Experiment satellites, but incorporates a number of improvements based on lessons learned, and features significantly increased complexity due to the accommodation of the laser ranging interferometer. This paper provides an overview of the challenging requirements levied on the observatory, and the mission and spacecraft design necessary to meet them. As the original Gravity Recovery and Climate Experiment spacecraft design has not been, to date, broadly discussed in the engineering literature, this paper further highlights original design rationales, where still applicable. As future satellite-based geodesy missions with similar constraints and challenges emerge, the implementation of the Gravity Recovery and Climate Experiment Follow-On observatory described herein can serve as a pathfinder and guide for the successful realization of these endeavors.

I. Introduction

IN THE past two decades, satellite gravity measurements have dramatically advanced our understanding of the processes that move mass above and below Earth's surface with broad applicability to the fields of oceanography, hydrology, and cryospheric and solid Earth sciences, among others. As Earth's gravity is affected by mass movement inside and on the surface of Earth, one can study the processes behind the movements by measuring gravity and its changes, both spatially and temporally. Satellite-based measurements enabled for the first time the measurement of a truly global and homogeneous gravity data set. This improved our understanding of the *mean* Earth gravity field (Fig. 1), resulting in improvements in the determination of permanent ocean currents [1] and in our understanding of solid Earth structure [2] and its effects on positioning and navigation. This also provided, for the first time, insights into the *time-variable* gravity field, shedding light on processes that vary on timescales from seasonal to decadal, including land water-cycle changes, ice sheets and glacier mass changes, sea-level changes, postglacial rebound, and postseismic changes, for example [3].

Starting with the onset of spaceflight, satellite trajectories were observed to deduce conclusions about Earth gravity field [4], as changes in the local gravity field act as disturbance to satellite trajectories, making them deviate from pure Keplerian orbits. In the following three decades, range and range-rate measurements to low-Earth orbiters were used to estimate time-average Earth gravity models. Techniques such as satellite laser ranging, Transit [5], DORIS (defined as Doppler Orbitography and Radiopositioning Integrated by Satellite) [6], and, finally, GPS, over time provided increasingly greater resolution for mean Earth model estimation. Time-variable gravity measurements, primarily derived using satellite laser ranging, were largely limited to the continental scales.

With the launch of the German CHAMP mission (short for Challenging Mini-Satellite Payload) in 2000, deviations of the satellite's orbit from the Keplerian orbit could, for the first time, be measured with centimeter accuracy continuously over the course of 10 years. In addition to a dual-frequency GPS receiver, CHAMP carried an accelerometer to measure the effects of atmospheric drag and solar and Earth radiation pressures, thereby allowing analysts to correct for their effects and produce large-scale static gravity fields of unprecedented accuracy [7].

In 2002, the U.S./German Gravity Recovery and Climate Experiment (GRACE) was launched, jointly developed by NASA and the German Aerospace Center (DLR) as part of NASA's Earth System Science Pathfinder Program [8]. Based on a measurement concept originally proposed by Wolff [9], the mission consists of flying two identical satellites in the same orbital plane at an average distance of 220 km (or about 30 s behind each other). Because of their in-plane separation, Earth's changing gravity field subjects the two satellites to different disturbance forces, with the accelerations applying first to the leading and then to the trailing spacecraft. For example, if flying over a massive mountain range, the leading satellite

Received 11 June 2018; revision received 22 October 2018; accepted for publication 1 January 2019; published online 26 April 2019.

*GRACE Follow-On Flight System Systems Engineer, Systems Engineering and Formulation Division. Associate Fellow AIAA.
†GRACE Follow-On MWI Instrument Manager, Communications, Tracking, and Radar Division.
‡GRACE Follow-On Deputy Project, Flight System and ACC Instrument Manager, GRACE-FO Project Office. Senior Member AIAA.
§GRACE Follow-On Project Systems Engineer, Systems Engineering and Formulation Division.
¶GRACE Follow-On LRI Instrument Manager, Communications, Tracking, and Radar Division.
**GRACE Follow-On Spacecraft Project Manager, Airbus Earth Observation Systems. Senior Member AIAA.
††GRACE Follow-On Science Team Member, Associate Professor, and Director, Center for Space Research. Associate Fellow AIAA.

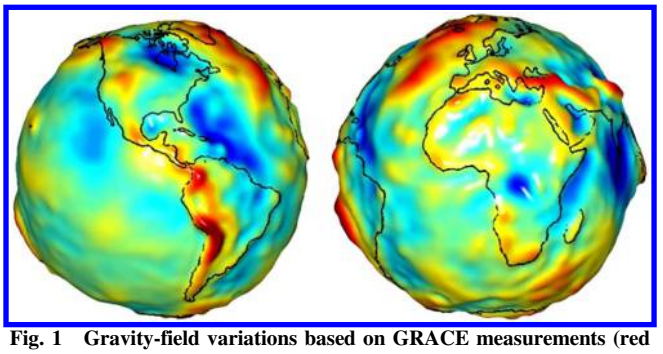

Fig. 1 Gravity-field variations based on GRACE measurements (red bulges: stronger gravity; blue depressions: weaker gravity).

is subjected to the mountain range's incremental gravitational pull first, thus accelerating toward the range and increasing the distance to the trailing satellite. Once the leading spacecraft passed the range, the same incremental gravitational pull is now decelerating it, while the trailing spacecraft is still accelerating toward the range. The leading and trailing satellites are thus accelerating and decelerating with respect to each other at different times during the overflight of the mountain range. The resulting changes in their relative distance are continuously measured with micrometer-level accuracy, i.e., to within a fraction of the width of a human hair using a microwave ranging instrument on each spacecraft, with both one-way range measurements containing the desired gravity-field information. Thus, the two spacecraft together act as a single observatory of gravity-field changes while they orbit Earth. In addition, just as for CHAMP, both satellites carry GPS receivers for precise positioning and timing, and accelerometers to measure and compensate for nongravitational disturbance forces. The monthly gravity-field snapshots provided by the GRACE mission provided the first detailed and accurate measurements of regional-scale mass variations everywhere on Earth.

With the unprecedented measurement accuracy of the GRACE observatory, both long-term and seasonal changes in the gravity field could be observed for the first time at spatial scales as short as 300 km. Diverse science results and accomplishments have been surveyed by several authors (e.g., Refs. [10,11]). These included seasonal changes in the water cycle of large river systems as well as longer-term trends, such as changes in water storage due to overusage of ground water for irrigation (Fig. 2), mass loss in the Greenland and the Antarctic ice sheets and the resulting rise in sea level, and the ongoing postglacial rebound [7]. GRACE measured gravity at a level of a few parts per million of the standard gravity of 9.81 m/s^2 at Earth's surface [12], and yielded gravity models that were improved by more than an order of magnitude at the long- and midwavelength compared to previous models [8]. Originally designed and built for a five year mission, the two spacecraft completed more than 15 years in orbit, before ending science operations in October of 2017 due to an age-related battery issue on one of the spacecraft.

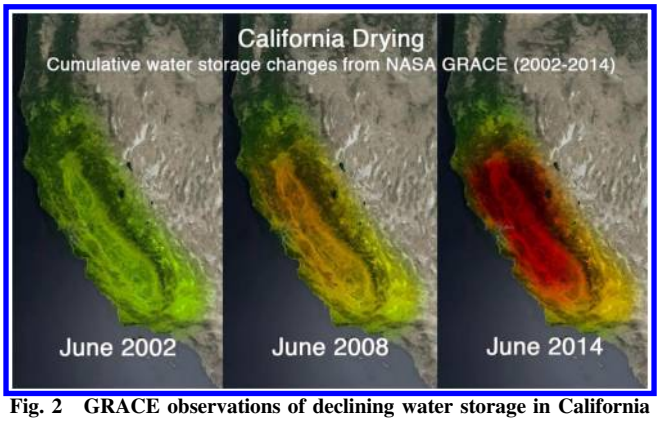

Fig. 2 GRACE observations of declining water storage in California (red represents greater accumulated water loss).

The same measurement concept used for GRACE was also successfully applied to map the lunar gravity field as part of the Gravity Recovery and Interior Laboratory (GRAIL) mission [13]. Each GRAIL spacecraft carried an X-band radio science beacon, allowing the use of the Deep Space Network (DSN) to determine each spacecraft's orbit, as well as an S-band time transfer system to synchronize the measurement times between both spacecraft. Unlike GRACE, the GRAIL spacecraft did not carry accelerometers due to the lack of an atmosphere around the Moon.

ESA's Gravity Field and Steady-State Ocean Circulation Explorer (GOCE) spacecraft launched in March of 2009 and was designed to collect information about the mean Earth gravity field to unprecedented resolutions. It carried a gradiometer consisting of six accelerometers, arranged pairwise along each axis. GOCE instruments provided measurements of gradients of gravity acceleration through differential accelerometry over a 1 m distance to the picometer/s^2 precision [14], thereby leading to estimation of time-average Earth gravity models with a spatial resolution of 100 km. To achieve this level of spatial resolution, GOCE's orbital altitude was chosen to be only about 260 km [15] with the resulting atmospheric drag and solar and Earth radiation pressures being continuously compensated for by an ion propulsion system. The mission lasted until November 2013, when GOCE's fuel was depleted and the spacecraft re-entered Earth's atmosphere.

In 2012, with GRACE well beyond its original lifetime, the joint U.S./German GRACE Follow-On (GRACE-FO) mission was conceived. Its objective is to provide continuity in the gravity-field observations beyond GRACE's lifetime. To save development time and cost, the GRACE-FO spacecraft and instruments (microwave ranging and accelerometer) were based on the original GRACE design. However, a laser ranging interferometer was added as a technology demonstration to serve as a pathfinder for future gravity mapping missions, making GRACE-FO the first-ever intersatellite interferometric mission (Fig. 3). As part of the joint U.S./German agreement, NASA is contributing the twin GRACE-FO spacecraft, the microwave instruments, the accelerometer, and part of the laser ranging interferometer, with the German Research Centre for Geosciences (GFZ) contributing the launch vehicle, the five year mission operations, and the remaining part of the laser ranging interferometer. NASA's Jet Propulsion Laboratory (JPL) manages the U.S. contributions for NASA and, in turn, contracted with Airbus Defence and Space to build the twin GRACE-FO spacecraft, and ONERA–The French Aerospace Lab to supply the accelerometer, based on their heritage of building the GRACE twin spacecraft and accelerometer, respectively. In addition to flying the laser ranging interferometer, a number of significant spacecraft modifications and upgrades are incorporated into the GRACE-FO design, both based on the lessons learned from GRACE as well as to accommodate part obsolescence since the original GRACE design.

This paper provides an overview of the GRACE-FO mission, spacecraft, and instruments, and details the differences to the original

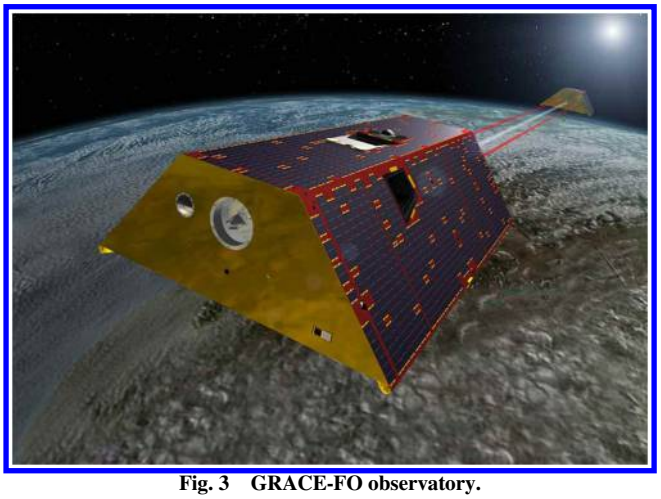

Fig. 3 GRACE-FO observatory.

Table 1 Science and instrument requirements

	Science requirements		
Long-term mean model	The long-term mean geopotential model shall be characterized by a spherical harmonic model to degree and order 150 or higher.		
Temporal variability	The temporal variability shall be characterized by sets of average values of the geopotential coefficients over 30 days or shorter, to spherical harmonic degrees 70 or higher.		
Geoid height error	Generate sets of 30 day average geopotential coefficients with an equivalent root mean square geoid height error measurement:		
	Harmonic degree	Geoid height error per degree, mm	Geoid height error cumulative, for $n > 2$, mm
	$n = 2$	< 0.10	— —
	$2 < n \leq 10$	< 0.01	< 0.02
	$10 < n \leq 70$	< 0.15	< 0.40
	$70 < n \leq 100$	< 1.50	< 3.50
	$100 < n \leq 150$	< 65.0	< 200
GPS sounding measurements	Acquire 200 GPS atmospheric profile soundings per day.		
	MWI requirements		
K/Ka-band phase measurement	Provide 10 Hz measurements of the K- and Ka-band carrier phases of the ranging signal received from the other satellite with a precision of 10^{-4} cycle.		
Temperature sensitivity (tone error)	Temperature sensitivity shall not exceed 2 μm (peak to peak) at twice per revolution (ionosphere free).		
Stochastic errors	Stochastic errors shall be below a PSD described by $2.62 * \text{sqrt}[1 + (0.003/f)^2]$ μm/sqrt (Hz).		
GNSS orbit determination	Provide GNSS data for orbit determination at a frequency of 0.5 Hz to better than 10 m (1-sigma).		
PPS timing	Provide a Pulse Per Second (PPS) signal to the spacecraft accurate to within ± 0.3 μs and traceable to GPS time.		
Velocity requirement	Provide velocity with accuracy better than 0.1 m/s (1-sigma) for each axis.		
	ACC requirements		
Measurement rate	Provide three-axis acceleration measurements at a rate of 10 Hz.		
Measurement ranges	The measurement range shall be a minimum of $\pm 5 \times 10^{-5}$ m/s^2 in the accelerometer Y and Z axes, and $\pm 5 \times 10^{-4}$ m/s^2 in the X axis.		
PSD noise in the X axis	$\text{sqrt}(\text{PSD}x) \leq 10^{-9} \times \text{sqrt}[1 + (f/0.5\text{ Hz})^4 + (0.1\text{ Hz}/f)]$ m/s^2/sqrt (Hz)		
PSD noise in the Y or Z axis	$\text{sqrt}(\text{PSD}y, z) \leq 10^{-10} \times \text{sqrt}[1 + (f/0.5\text{ Hz})^4 + (0.005\text{ Hz}/f)]$ m/s^2/sqrt (Hz) for 5×10^{-5} Hz $< f <$ 2.5 Hz		
Maximum error tones	The maximum error tones shall be less than or equal to 4×10^{-12} m/s^2 for the Y and Z axes, and 5×10^{-10} m/s^2 for the X axis from 50 μHz to 0.1 Hz.		
	LRI requirements		
Measurement rate	Provide ~10 Hz measurements.		
Stochastic error	Changes in the separation between a reference point on each laser interferometer shall be measured with the following: $x(f) < 80$ nm/sqrt(Hz) $*$ NSF(f) for $\text{NSF}(f) = \text{sqrt}[1 + (f/3\text{ mHz})^{-2}] * \text{sqrt}[1 + (f/10\text{ mHz})^{-2}]$ for 2 mHz $< f <$ 0.1 Hz		
Deterministic error	Contribution to deterministic errors shall not exceed 2 μm amplitude for harmonics of the orbital frequency between $10 \leq n \leq 200$.		

GRACE mission. However, as the original GRACE spacecraft design (to the best of the authors' knowledge), has not been, to date, broadly discussed in the engineering literature, this paper, in addition, highlights the original GRACE design rationales, where applicable. Accordingly, the paper is organized as follows: Sec. II outlines the GRACE-FO science requirements and mission concept. Next, Sec. III discusses the GRACE-FO instruments, including the microwave ranging instrument, the accelerometer, and the laser ranging interferometer. Section IV then reviews the GRACE-FO spacecraft design, outlining its commonalities and differences to the original GRACE spacecraft as well as rationalizing design decisions, then and now. Section V discusses mission operations, and Sec. VI, finally, provides the conclusions.

II. Science Requirements and Measurement Concept

A. Science Requirements

Earth's gravitational potential can conveniently be expressed in terms of spherical harmonic coefficients. Consequently, the science requirements for GRACE and GRACE-FO missions were stated as requirements on the accuracy and the degree to which the coefficients have to be determined. The mathematical models and numerical methods needed to relate the accuracy of the geopotential's spherical harmonic coefficients to the various mission and spacecraft system error contributions were well known [3], making this representation convenient for trade studies needed for mission architecture development.

In general, spherical harmonic representation to maximum degree N is needed for the representation of geographical features at spatial scales of approximately $20,000/N$ km. Thus, targeting time-variable gravity measurements down to a spatial scale of 300 km necessitated placing an accuracy requirement on the determination of the geopotential spherical harmonics to degree 70. To ensure representation of the variations at the seasonal and climate timescales and at these spatial scales with adequate global ground-track coverage, these requirements were placed on the 30 day average representation of Earth's gravity model. For oceanographic applications, however, the determination of the time-average model of the Earth gravity field to spatial scales less than 200 km was desirable, thus leading to accuracy requirements up to spherical harmonic degree and order 150 for the mean Earth gravity-field model. To make the geopotential harmonic requirements physically more meaningful, the spherical harmonic error requirements were stated in terms of their contribution to the total global root-mean-square geoid height error—a quantity that is easily convertible to water height or mass or gravity units [3].

GRACE-FO's science requirements are specified in Table 1. They are identical to GRACE's science requirements and call for the generation of both a long-term mean gravity model up to degree 150 as well as a temporally variable gravity model up to degree 70 averaged over 30 days. Both a geoid height error per degree as well as a cumulative height error starting at degree 3 are specified.

In addition to the monthly gravity maps, GRACE-FO also is required to measure 200 Global Positioning System (GPS) radio occultation measurements of Earth's ionosphere and atmosphere every day using the microwave instrument's GPS radio occultation antenna. These profiles will be used to determine temperature distributions and water vapor content in support of weather forecasting.

B. Orbit Selection

The measurement sensitivity of a gravity mapping mission depends on its orbital altitude, with a lower altitude providing higher

Table 2 Gravity-field measurement error breakdown

Measurement	Error breakdown
Intersatellite ranging measurement	Thermal distortions
	Center of mass motion
	Thermally induced tone errors in MWI/KBR
	Thermally induced noise error in MWI/KBR
	Multipath errors in KBR horn antenna
	MWI phase flatness
	Attitude knowledge error:
	Star tracker to ACC ground alignment knowledge uncertainties
	Star tracker to ACC in-flight stabilities
	Star tracker performance
	Reference pointing knowledge
	LRI range measurement tone error
	LRI range measurement noise error
Nongravitational acceleration measurements	ACC unit measurement noise
	ACC unit tone errors
	ACC unit scale factor and bias error
	ACC to CoM ground alignment
	ACC to CoM in-flight stability
	Attitude knowledge error:
	Star tracker to ACC ground alignment knowledge uncertainties
	Star tracker to ACC in-flight stabilities
	Star tracker performance
Precision orbit determination	GPS positioning accuracy
	GPS velocity measurement accuracy
	GPS timing accuracy

sensitivity to, and thus a greater spatial resolution of, the gravity field. On the other hand, lower orbital altitudes lead generally to lower mission lifetime due to the increased atmospheric drag. For climate and Earth system science applications, a long time series of measurements is required, and flying a higher orbital altitude mission over several years is thus preferred. In such an orbital configuration, longer spatial wavelengths in the gravity field could be well observed and resolved over a long mission duration, with the ongoing natural decay in orbital altitude enabling shorter wavelength to be observed toward the end of the mission [3].

The 500 km orbit selected for the GRACE mission, in the atmospheric drag environment anticipated for its lifetime, offered the best opportunity to monitor the time-variable gravity field for the long duration needed to conduct climate science [12]. The near-polar inclination of 89 deg ensured global coverage while allowing for the needed launch mass. The low orbital eccentricity of 0.005 ensured that the two satellites had matching eccentricities to reduce the sensitivity of gravity-field measurements due to altitude changes over the course of an orbit, and to minimize the spacecraft attitude excursions necessary to keep the two spacecraft pointing at each other. The selection of the average intersatellite separation was driven by a trade between signal attenuation and observability of the largest-scale geophysical signals. At smaller separations, signals are smaller, but more precise measurements can be made. At larger separations, signals are larger, but ranging precision is reduced. To this end, an average spacecraft separation of approximately 2 deg, or 220 km $\pm$ 50 km, was selected to ensure observability of spherical harmonics in the range of interest, as explained in Ref. [12] in more detail. The spacecraft separation is allowed to vary between 170 km and 270 km as a compromise between the operational complexity of keeping the spacecraft in the desired distance range and uniformity in the quality of gravity measurements.

To limit the required fuel usage over the course of the mission, the ground track and the resulting ground coverage were not actively controlled. Instead, the orbits of both satellites are left to naturally decay, which ensures a varying ground track most of the time. (At certain orbital altitudes, ground-track repeat conditions, can, however, manifest themselves as explained in Ref. [12] in more detail.) After five years of operation, the GRACE satellites decayed to an orbital altitude of 466 km, and in May 2017, after 15 years of operation and shortly before their decommissioning, the satellites had reached an altitude of 335 km. To achieve the stated mission requirements, GRACE-FO will fly in a similar orbit as GRACE.

C. Measurement Concept and Error Breakdown

As for the original GRACE mission, the GRACE-FO measurement concept is based on the use of a dual-frequency K/Ka-band microwave ranging system to measure the distance changes between the satellites. With both satellites pointing to each other, each spacecraft is transmitting and receiving a dual-frequency microwave signal, and the four one-way phase measurements are used in ground processing to produce a distance change measurement that is corrected for errors induced by the ionosphere as well as onboard oscillator instabilities [16].

The satellites experience changes in their intersatellite range due to nongravitational forces as well. These nongravitational contributors include atmospheric drag, solar and Earth radiation pressures, and residual imbalanced thruster firings for attitude control by both satellites. Using the onboard accelerometer on each spacecraft, the effects of all nongravitational accelerations are measured and then corrected in the data analysis. Finally, the onboard GPS receiver provides precise timing and position information needed for the data analysis.

The scientific data-analysis concept is based on the analysis of the disturbance of the satellites' trajectories from previously well-understood models. Extensive prior knowledge and mathematical models exist for gravity-field variations due to nonuniformities in Earth's mean field, and time variations due to lunisolar perturbations, Earth and ocean tides, and atmospheric pressure and oceanic variability. Models for such processes, together with observations of nongravitational accelerations, are used to predict the satellites' positions and velocities, and therefore, the relative distance changes between them. The deviations between the predicted and the actual distance change measured by the microwave ranging instrument are the results of processes for which we do not have a priori models. By aggregating these residuals every month, and assuming a piecewise constant correction to the gravity-field model over this period of time, an updated monthly gravity field is determined, which represents a new measurement of the variations in the water cycle, changes in ice sheets, and/or other deficiencies in the a priori models.

The contributors to the errors in the estimated geopotential parameters fall into one of four domains: 1) intersatellite ranging measurement errors, 2) nongravitational acceleration measurement errors, 3) precision orbit determination errors, and 4) temporal and spatial undersampling and dealiasing errors. The contributors for the first three domains are shown in Table 2.

The intersatellite ranging measurement is affected by temperature changes as the spacecraft enter and exit eclipses due to both the thermo-mechanical expansion/contraction as well as possible temperature sensitivity of instrument errors. As such, these errors occur at orbital frequencies and directly affect the measurement of interest. Similarly, spacecraft center of mass motion over time and attitude and pointing knowledge affect the ability to determine the distance between the spacecraft center of mass and the ranging instruments, and thus will contribute to the ranging error. The attitude knowledge error, in turn, is in large part dependent on the ability to measure the orientation of the star trackers during the ground alignments, the stability of that alignment in flight, and the star tracker performance itself. Finally, instrument noise and multipath errors in the microwave horn antenna have to be accounted for as well.

The nongravitational acceleration measurements are performed by the onboard accelerometers. Instrument measurement noise as well as thermally-induced tone errors occurring at orbital frequencies limit the ability to subtract out nongravitational effects from the measured range measurement. Next, errors in the ground alignment of the accelerometer relative to the actual spacecraft center of mass, as well as the migration of the center of mass over time, lead to a coupling of spacecraft rotational accelerations into the linear acceleration measurements of interest. The center of mass migration is due to the thermo-elastic expansions/contractions occurring at orbital frequencies as well as differential fuel usage across the spacecraft cold-gas propulsion system over time. As for the ranging measurements, attitude knowledge errors limit the ability to transform the acceleration measurements, observed in the spacecraft frame, into an inertial frame necessary for the generation of gravity fields.

The precision orbit determination is limited by the onboard GPS receiver's positioning, velocity, and timing measurement accuracy, as well as the ground control team's orbit determination processes.

Whereas the intersatellite ranging and acceleration measurements and precision orbit determination are primarily a function of the gravity mapping observatory implementation, the last error contributor, undersampling and dealiasing, is a result of the observatory's limitation in measuring all of Earth's processes affecting the gravity field with the necessary temporal and spatial resolution. Rapid Earth gravity-field variations, at timescales less than 30 days, are not adequately sampled and can cause aliasing in the 30 day mean Earth gravity-field estimate. The aliasing error is mitigated either through the use of precise, independently derived models of short-period geophysical variations, or through data processing strategies. This class of error contributors is subject of intensive ongoing research in the geodesy community [3] and is beyond the scope of this paper.

On the other hand, the instrument and spacecraft implementations employed for GRACE-FO to minimize the first three error components are the subject of the rest of this paper. In particular, instrument and spacecraft thermal control, structural alignments and in-flight stability, center of mass migration and control, as well as attitude knowledge and pointing control are paramount aspects in addressing the challenges of gravity-field measurements and in implementing a gravity mapping observatory, and are addressed in the next two sections.

III. Instruments

As a continuation mission to GRACE, GRACE-FO will fly a microwave ranging instrument, called the Microwave Instrument (MWI), and an accelerometer (referred to simply as the ACC), similar or identical to ones previously flown on GRACE. The MWI has also previously flown on the GRAIL mission, which mapped the inner structure of the Moon [13]. The ACC is an improved version of the one originally flown on GRACE, as outlined below. Also, as for GRACE, a laser retroreflector (LRR), supplied by GFZ, is mounted on the nadir side of both GRACE-FO spacecraft for ground-based laser ranging and orbit determination. It is entirely passive and consists of four corner-cube prisms mounted on four sides of a pyramid. However, in a notable departure from the GRACE mission, GRACE-FO will also fly a laser ranging interferometer (LRI), also referred to as Laser Ranging Instrument, as a technology demonstration for future gravity mapping missions. The MWI, ACC, and LRI are explained next in greater detail. The LRR will not be further discussed.

A. Microwave Instrument

The MWI is the primary instrument on the two GRACE-FO spacecraft, used to measure the temporal difference in range between the two orbiters using 24 GHz K- and 32 GHz Ka-band cross-links, and to provide GPS position, velocity, and timing information. The use of a dual-frequency approach allows the calibration and removal of ionospheric effects on the measurements of interest. The Dual-One-Way Range (DOWR) measurements for both spacecraft and frequencies are downlinked and postprocessed to ultimately provide the time series of Earth gravity-field maps. The four phase measurements are hereby combined to yield a signal that is proportional to the distance rate change between the satellites with phase variations due to long-term clock instabilities canceled out [16].

The key performance requirements are listed in Table 1. To accommodate the science requirements of detecting gravity-field components at the scale of a few hundred kilometers, the range must be measured to an accuracy of a few micrometers (10^{-6} m), which, for the 24 and 32 GHz ranging signals, corresponds to approximately 10^{-4} cycles. Furthermore, the update rate is required to be (at least) 10 Hz to minimize errors when interpolating the measurements to the correct epoch time. The thermally induced tone errors (i.e., the thermoelastic effects on the range measurements) cannot exceed 2 μm for twice the orbital frequency component. To allow orbit and attitude as well as overall spacecraft time determination, the MWI GPS receiver has to provide position and velocity information at an update rate of 0.5 Hz, and accuracy of 10 m and 0.1 m/s, respectively, and a pulse-per-second time signal accurate to ± 0.3 μs. In most cases, the requirements were carried over from GRACE, but in some cases, the project has tightened requirements to closer meet GRACE actual performance rather than requirement.

As for GRACE, the MWI is a NASA JPL–developed instrument. It consists of a K/Ka-band Ranging Assembly (KBR), block-redundant Ultrastable Oscillators (USOs), block-redundant Instrument Processing Units (IPUs), and a set of three GPS antennas and low-noise amplifiers (LNAs), cross-strapped to the IPUs. The KBR assembly, in turn, contains block-redundant Microwave Assemblies (MWAs) for the 24 GHz K- and 32 GHz Ka-band transmitter and receiver chains that are cross-strapped to a single horn antenna via splitters and a waveguide switching matrix. Figures 4 and 5 show the KBR assembly and the functional block diagram of the MWI, respectively.

The MWI functional architecture is identical to the one on GRACE (see Ref. [10]), and many of the performance-driving components are built to the same specifications as the ones for GRACE and/or GRAIL, although in a few cases, updates to the design were done, where applicable, to mitigate schedule, cost, and performance risk, or to adapt to the adopted GRACE-FO sensor and computing architecture. Whereas for GRACE the two spacecraft star cameras were functionally connected to the IPU, with the IPU responsible for processing the star images to obtain spacecraft attitude, for GRACE-FO the star trackers process their images and are directly interfacing with the onboard computer, and thus, are no longer part of the MWI and IPU architecture. The MWI redundancy architecture was updated from internally redundant IPU and signal processing units on GRACE to block-redundant IPUs on GRACE-FO.

Each satellite has a redundant pair of USOs, with an approximate Allan deviation of 10^{-13} at 1 s time interval, providing the coherent frequency references for the MWA and IPU. The USO frequencies of both spacecraft are slightly offset from each other to obtain the radio-frequency (RF) mixing products in the desired measurement baseband frequency at the IPUs, and subsequently in the required science data. The USOs additionally provide a reference for the LRI instrument.

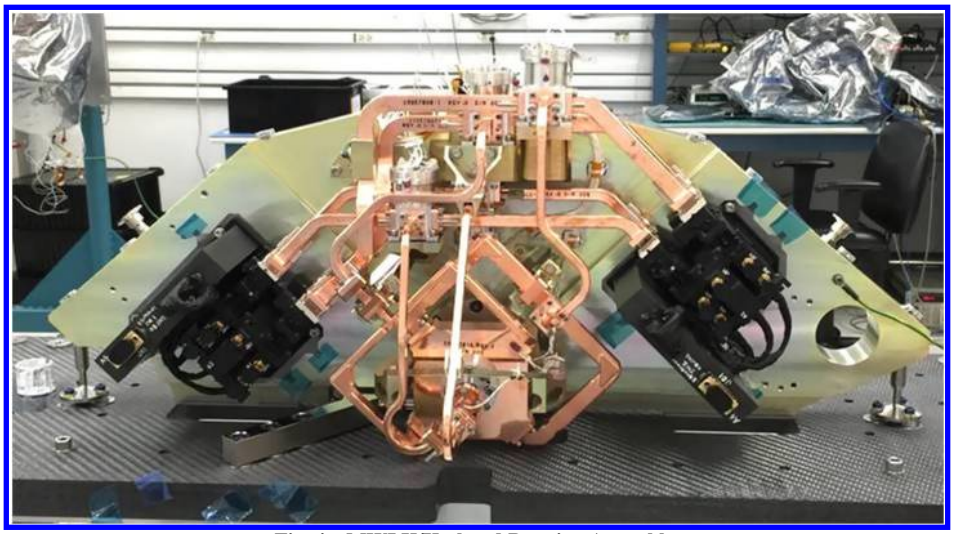

Fig. 4 MWI K/Ka-band Ranging Assembly.

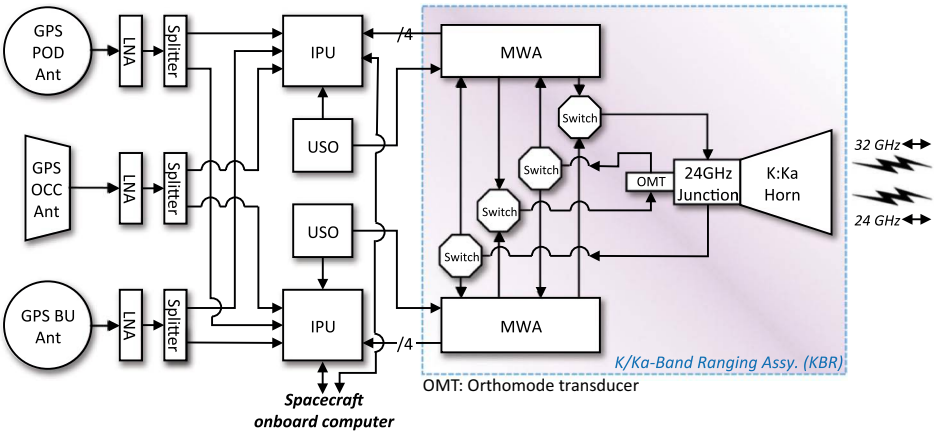

Fig. 5 MWI block diagram.

The KBR provides the RF front end to the measurement system. The dual-band, dual-linearly polarized horn antenna, the waveguide feeds, and the redundant MWA K/Ka-band 24 and 32 GHz transmitters and receivers are all mounted on a dedicated KBR structure (see Fig. 4). The horn antenna is near built to print from the GRACE design, with a few modifications to the aperture cover and the feed components. The MWAs up-convert the USO signal to K- and Ka-band for transmission, as well as down-convert the received K- and Ka-band signals to baseband orthogonal In-phase and Quadrature (I/Q) signals.

The IPU receives and digitally samples the MWA baseband I/Q signals. These measurements are the basis for the DOWR measurements. The IPU contains the GPS receiver providing navigation and orbit determination information, time reference, and correlation of data products, as well as ancillary Earth limb radio occultation measurements. The GPS receiver can track up to 16 GPS satellites for positioning and 4 for radio occultation measurements. The IPU design was updated based on the evolving line of Global Navigation Satellite System (GNSS) receivers at JPL, and to account for the different onboard computer interface, parts obsolescence, and integration of a reprogrammable FPGA signal processor.

As for GRACE, the MWI GPS antenna suite comprises three antennas operating at L1/L2 GPS frequencies, specifically, the precision orbit determination (POD) antenna, the occultation (OCC) antenna, and the backup (BU) antenna. However, for GRACE-FO, the system is also being designed to accommodate GNSS signals, including the GPS L5 channel. The POD antenna is mounted in the zenith direction on the spacecraft and receives GPS signals for precision orbit determination; these signals are also used to provide local position and velocity solutions for the spacecraft's attitude control system. The OCC antenna is mounted on the opposite side of the spacecraft as the K/Ka-band antenna and measures the signal of GPS signals near Earth's limb, resulting in observations of the ionosphere and atmosphere. These signals are used to provide data for weather, climate, and ionospheric predictions. Finally, the BU antenna is located on the same panel as the OCC antenna, and would be used as backup in case the primary precision orbit antenna fails.

B. Accelerometer

The accelerometers (ACCs) are used to measure nongravitational accelerations on the spacecraft to separate their effects on the spacecraft center of mass from the effects of gravitational accelerations, which are the measurements of interest. The nongravitational accelerations include residual imbalanced thruster firings, and nongravitational environmental effects, such as atmospheric drag and solar and Earth radiation pressures. To minimize the coupling of rotational accelerations on the ACC measurements, the ACC is placed such that its proof mass is at the spacecraft center of mass. The key performance requirements are listed in Table 1.

The ACC for GRACE-FO is supplied by ONERA in Paris, France, and is specially designed to measure weak accelerations for space applications. The GRACE-FO ACC is based on a lineage of accelerometers previously flown on the German CHAMP and ESA's GOCE geodesy missions, and is similar to the one flown on GRACE, but with some improvements as outlined next. References [17–19]

provide additional background information and implementation details.

The measurement principle is based on the electrostatic suspension of a proof mass within a cage made up of six pairs of electrodes. The latter serve both as capacitive sensors and electrostatic actuators. Any nongravitational acceleration on the spacecraft displaces the cage with respect to the proof mass (whereas gravitational acceleration affects both the cage and the proof mass in the same way, and thus is not detected). In their function as sensors, the electrodes measure the instantaneous position of the proof mass within the cage, as the measured capacitance varies with the distance of the proof mass to the electrodes. The sensed displacement signal is sent to a PID (proportional–integral–derivative) controller, and a control voltage is applied to the electrodes in their function as electrostatic actuators to recenter the proof mass. A thin platinum wire supplies the proof mass with the required constant polarization voltage. The use of six pairs of electrodes and associated servo channels results in the proof mass being a drag-free acceleration sensor in all six degrees of freedom, thus providing linear and angular acceleration in all three axes derived from the control voltages applied to keep the proof mass centered within the cage. Figures 6 and 7 show the ACC sensor unit and the functional block diagram of the ACC, respectively.

The proof mass is a parallelepiped made of titanium alloy and weighing 72 g, and the electrode cage is made up of gold-coated silica with an ultralow coefficient of expansion. The sensor assembly is enclosed in a housing and sole plate, and a getter is employed to maintain vacuum conditions.

A number of improvements have been made to the GRACE-FO sensor unit compared to its precursor unit on GRACE. First, the gold wire attached to the proof mass of the GRACE ACC has been replaced by a platinum wire to increase tensile strength. Next, to minimize the susceptibility to thermal fluctuations and electromagnetic interference, the position sensing and control loop electronics, the analog-to-digital conversion circuitry, and all associated signal

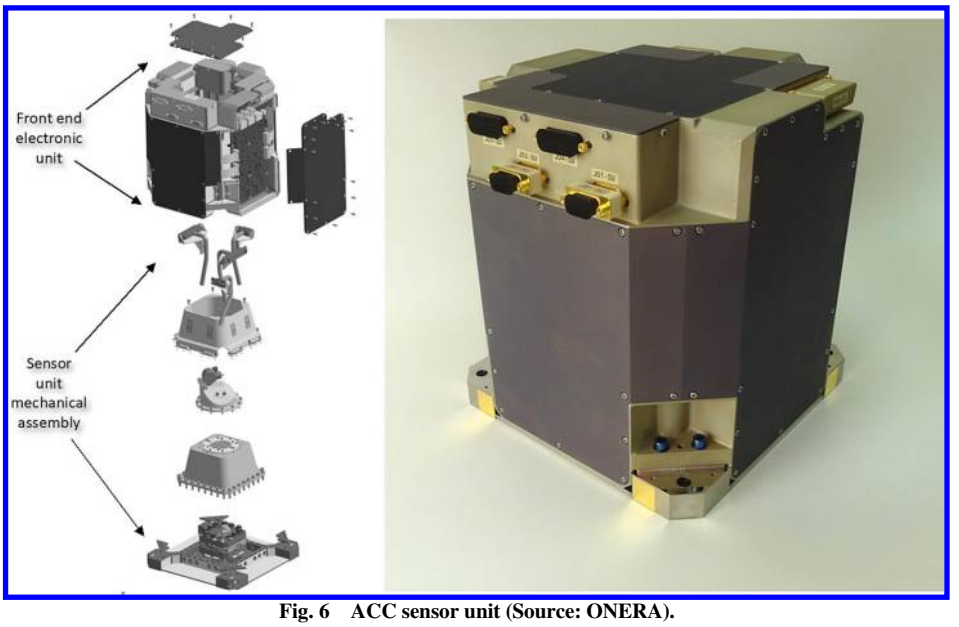

Fig. 6 ACC sensor unit (Source: ONERA).

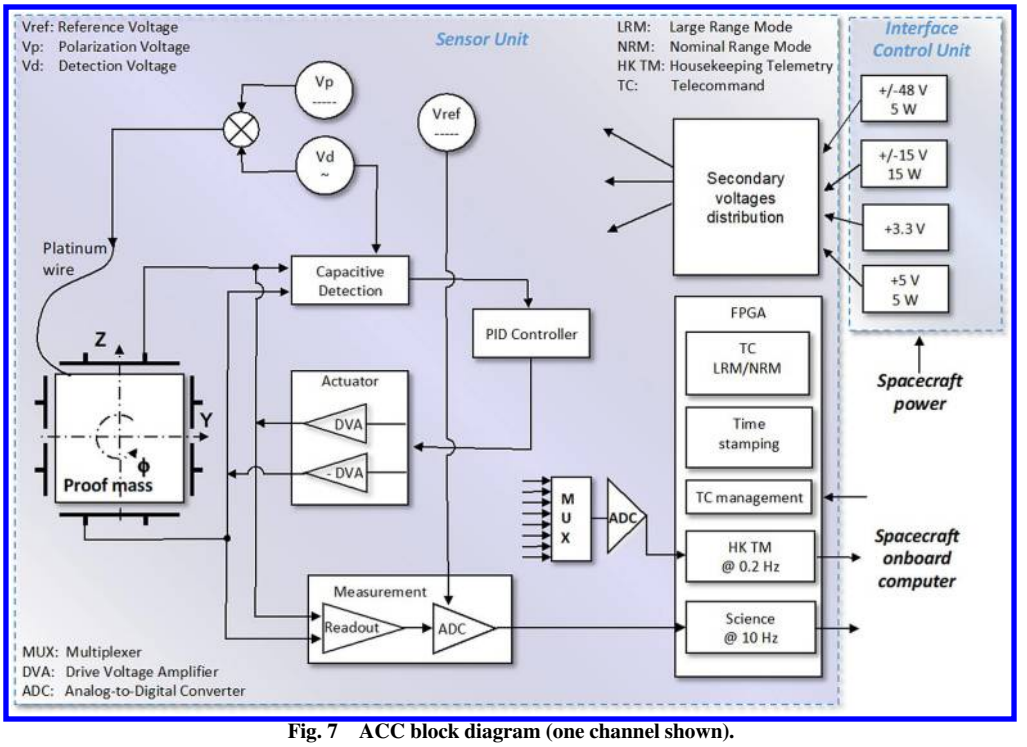

Fig. 7 ACC block diagram (one channel shown).

condition logic and voltage references have been collocated with the sensor unit in the same thermal enclosure. A field-programmable gate array (FPGA) is used to control the sensor operations and provide the digital interfaces to the spacecraft computer over the nominal and redundant data bus. The latter electronics are packaged into four boxes that surround the mechanical sensor unit described earlier, and the combined assembly is referred to as the sensor unit (SU).

A second unit, the interface control unit (ICU), performs power conversion using the primary regulated power supplied to it and providing secondary voltages to the sensor unit. In addition, it houses the getter power supply; the latter is driven by ground-support equipment via a skin connector and is operated occasionally to maintain vacuum. The interface control unit is attached to the sensor unit via a separate harness, but it can be mounted at a distance from the sensor unit.

The three accelerometer axes have different characteristics, as the accelerometer X axis is designed to withstand the high voltages necessary to suspend the proof mass under 1 g Earth gravity. This allows the accelerometer Y and Z axes to be tested on the ground, but results in the X-axis tone error (and noise performance) to be more than the other two axes. Consequently, the achieved acceleration tone errors are 1.64×10^{-10}, 2.96×10^{-12}, and 2.49×10^{-12} $\mathrm{m/s^2}$ for the X, Y, and Z axes of one ACC unit, and 1.53×10^{-10}, 2.64×10^{-12}, and 2.78×10^{-12} $\mathrm{m/s^2}$ for the other ACC unit, respectively. In flight, the ACC X axis will be oriented along the spacecraft Y axis (normal to orbit plane), as it requires the least precision, whereas the two ACC precision axes are used to measure the in-plane components of the nongravitational force measurements (along track and radial) [12].

C. Laser Ranging Interferometer

The laser ranging interferometer (LRI) was added to the GRACE instrumentation as a technology demonstration in support of future gravity mapping missions. Like the MWI, it measures fluctuations in the separation between the spacecraft, with the expected sensitivity improved by a factor of 50 compared to the MWI. It will be the first intersatellite interferometer flown in space. The LRI benefits from technology and design developments in the United States and Germany for the Laser Interferometer Space Antenna (LISA), a space-based gravitational wave detector currently under development as an ESA-led mission, as well as from technology investments targeting improved geodesy missions. The hardware complement on the two spacecraft are identical. On one spacecraft, commanded from the ground to be the "master" laser, frequency-stabilized light is sent to the distant spacecraft. On the distant spacecraft, an interferometric beat note between the incoming and local laser light is used to offset phase-lock the local laser, whose light is sent back to the master spacecraft. Phase measurements are recorded on both spacecraft, just as for the MWI, but the measurement on the master spacecraft corresponds to the round-trip change in separation of the two spacecraft. The performance of the LRI is dominated by residual laser-frequency noise. The development and implementation of the LRI are a joint U.S.–German collaboration and are further detailed in Refs. [20,21].

The stated performance requirements for the GRACE-FO LRI are shown in Table 1. In addition to the performance requirements stated earlier, the LRI has to be designed not to interfere with the existing GRACE-FO instrumentation. In an ideal implementation, the optical axis of the LRI would be placed on or near the line connecting the center of mass of both spacecraft (when pointing at each other), as any offset from this line increases the coupling of spacecraft attitude jitter into the desired distance measurement. However, just like for the original GRACE spacecraft, the MWI KBR assembly and horn are placed on this axis, as well as one of the cold-gas propulsion system tanks. Moreover, the accelerometer proof mass is already placed at the center of mass location as detailed earlier. To accommodate these constraints and still minimize any undesired coupling of spacecraft attitude jitter, the LRI relies on a symmetric off-axis configuration using a Triple Mirror Assembly (TMA) to route the incoming and outgoing laser beams around the MWI KBR assembly and propulsion tank in a racetrack configuration.

In this arrangement, the TMA is effectively a corner-cube reflector, whose three perpendicular mirrors have been split up to create an extended corner cube. This arrangement routes the optical path around the MWI and propulsion hardware. Moreover, the effective vertex of the corner cube formed by the three mirrors lies outside of the TMA assembly, and can therefore be placed to coincide with the accelerometer proof mass and spacecraft center of mass. This, in turn, allows the LRI to measure the changes in the round-trip path length between the centers of mass of both spacecraft over time. Figures 8 and 9 show the LRI components and the functional block diagram of the LRI, respectively.

In addition to the TMA, the LRI consists of 1) a laser source, 2) a Laser Frequency Cavity Assembly used to stabilize the laser frequency, 3) an optical bench assembly and associated optical bench electronics performing the interference measurement with the incoming beam and pointing the outgoing laser beam, 4) baffles and light path closures providing protection and containment of the laser light as well as thermal insulation, and 5) a laser ranging processor controlling all functions of the LRI and outputting the interference measurements.

The laser source (LAS) provides the laser beam required to perform the laser interferometry. It has a wavelength of 1064 nm and an output power of approximately 25 mW. Most of the light power is routed to the optical bench assembly to be used as the outgoing beam to the other spacecraft, with the remainder used for laser-frequency stabilization in the cavity.

Similar to the required use of the USO in the MWI ranging measurement, laser-frequency stabilization using the cavity (CAV) is necessary, as changes in laser frequency cannot be distinguished from changes in spacecraft distance, and any residual error in stabilization will thus manifest itself as an error in the science measurement. To this end, the ability to stabilize the laser frequency is expected to limit the LRI measurement accuracy that is ultimately achieved. The stabilization approach relies on the Pound–Drever–Hall technique, and the cavity performance is critically dependent on its internal temperature stability and vacuum level. In support of the latter, the cavity is implemented with a vent tube to the outside of the spacecraft.

Laser light is routed via optical fiber to the optical bench assembly (OBA). A small amount of light passes through a beam splitter to act as local oscillator for the light received from the distant spacecraft, while the rest of the light is routed through the TMA to the distant spacecraft. Beam pointing is controlled using a steering mirror with a small signal bandwidth of 2 kHz. During the initial acquisition sequence of the LRI, the mirror is used to scan for the distant spacecraft. Once the instrument has acquired it, the steering mirror is required to maintain track of the other spacecraft, as the fluctuations in the spacecraft pointing (dead-banding) are larger than the beam convergence of the outgoing beam. (The MWI beam width is sufficiently large to accommodate the expected spacecraft attitude fluctuations.) The OBA further combines the incoming light from the other spacecraft with the local laser light to form a (heterodyne) beat note whose phase is detected by a redundant quadrant photoreceiver (QPR) in the OBA. This phase signal represents the measured change in spacecraft distance and is sent to the laser ranging processor, which extracts the actual phase measurement. In addition to the phase signal, the quadrant photoreceiver also uses differential wavefront sensing (DWS) to measure the misalignment between the incoming and outgoing beams. This information is then used in the laser ranging processor to compute a correction signal that is sent to the two-axis steering mirror in the OBA to correct the misalignment of the outgoing beam. The optical bench electronics (OBE) provide power and signal conditioning to the photoreceiver, as well as power and driver/sensing electronics for the steering mirror.

From the OBA, the outgoing laser beam is transmitted to the TMA, which routes it around the cold-gas tank and microwave instrument. Correct TMA alignment is thus fundamental to ensure that the outgoing beam stays pointed to the distant spacecraft. The TMA consists of a carbon-fiber-reinforced polymer (CFRP) hollow tube of 600 mm length as the TMA mechanical frame, a CFRP bracket as the main interface point, and two mirror assemblies made of ZERODUR on each end of the tube. The input side of the TMA holds a single

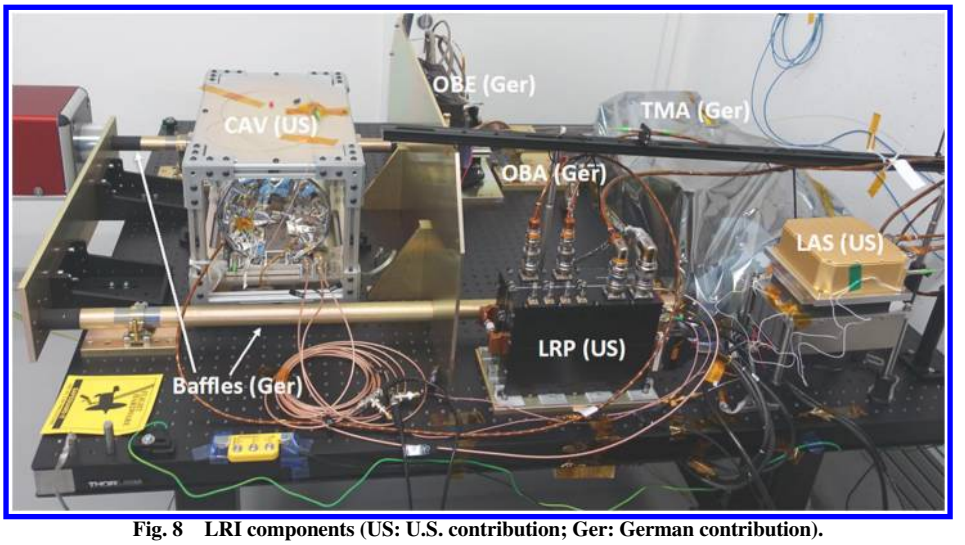

Fig. 8 LRI components (US: U.S. contribution; Ger: German contribution).

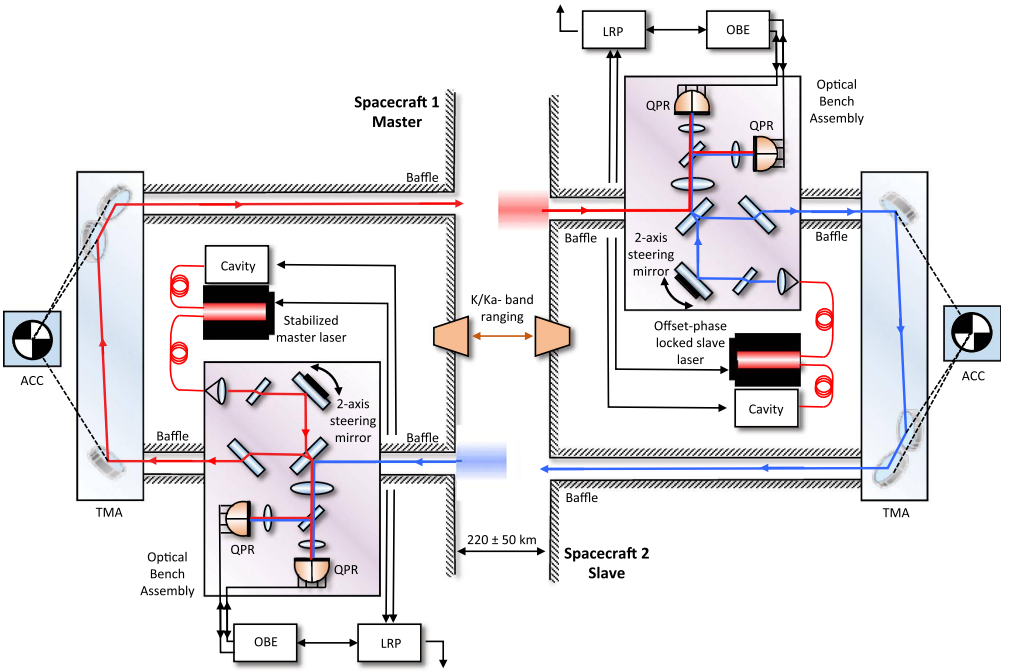

Fig. 9 LRI block diagram.

mirror, whereas the outgoing side contains the other two. Because of its low coefficient of thermal expansion, the TMA CFRP tube contributes to the stability of the beam path.

The incoming and outgoing laser beams are accommodated by two round openings in the spacecraft front panel. The laser-beam path through the satellite is enclosed by baffles along the spacecraft *X* axis, and by light path closures on each side of the TMA-to-baffle interfaces. The enclosures serve multiple purposes. On the one hand, they ensure that no spacecraft hardware accidentally blocks the beam path, help reduce the effects of stray light on the interferometer, and minimize contamination of the TMA optical surfaces during integration and from outgassing later in orbit. On the other hand, they protect the satellite's interior against atomic oxygen entering the opening in the front panel, as well as provide thermal isolation from the effects of pointing the openings into the sunlight or to deep space. Furthermore, they provide improved personnel safety against laser stray light during the integration campaign.

The laser ranging processor (LRP), finally, has a number of primary functions. It measures the phase of the laser interferometer signal detected by the OBA photoreceiver, and provides the measurements, representing the change in distance between the two spacecraft, to the spacecraft onboard computer for future downlink. The laser ranging processor further controls the local laser frequency either by stabilizing it using the cavity frequency reference (master mode) or by phase-locking it to the frequency of the incoming beam (slave mode). The processor also uses differential wavefront sensing on the quadrant photoreceiver to keep the outgoing light parallel to the incoming light using the steering mirror on the optical bench. Finally, during the acquisition of the distant spacecraft, the laser ranging processor performs the search required to establish the optical link using the directional information to the other spacecraft, which it receives from the spacecraft onboard computer.

Unlike the MWI, the LRI is a technology demonstration and is only required to operate for the first year. As such, the LRI is implemented as a single-string instrument with limited redundancy, including redundant quadrant photoreceivers, redundant laser pump diodes, and a cavity on each spacecraft, with only one required for operation.

IV. Spacecraft

As outlined in previous sections, the key GRACE-FO spacecraft challenges and corresponding key requirements lie in the areas of thermal control, structural alignments and in-flight stability, center-of-mass control, attitude knowledge, and pointing control. Moreover,

the thermal control and structural stability are inherently coupled in that the thermal variations will lead to structural bending and distortions. With the exception of LRI accommodation requirements, which have been newly added for GRACE-FO, most of the key requirements have been inherited from the original GRACE mission, although refined in some instances.

The GRACE-FO spacecraft are based on the mechanical, thermal, and propulsion design of the original GRACE spacecraft [22,23], but, due to part obsolescence, use the command and data handling, power, and sensor architecture of the ESA Swarm spacecraft launched in 2013. However, a number of key lessons learned from the extensive GRACE flight experience were incorporated into the GRACE-FO spacecraft design, and the addition of the LRI resulted in a modified spacecraft layout and increased complexity compared to the original GRACE spacecraft layout (see Figs. 10–12) [24]. This section discusses the general GRACE-FO spacecraft layout, and details the

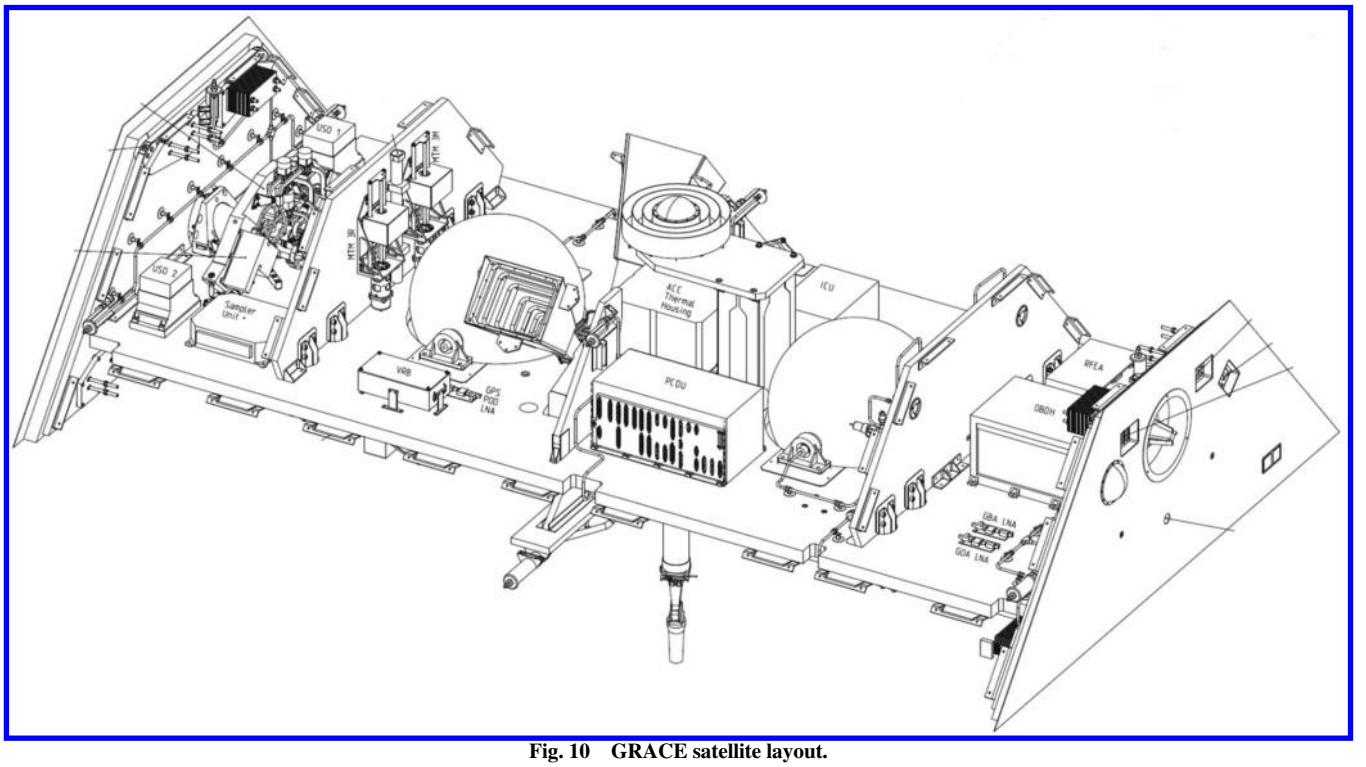

Fig. 10 GRACE satellite layout.

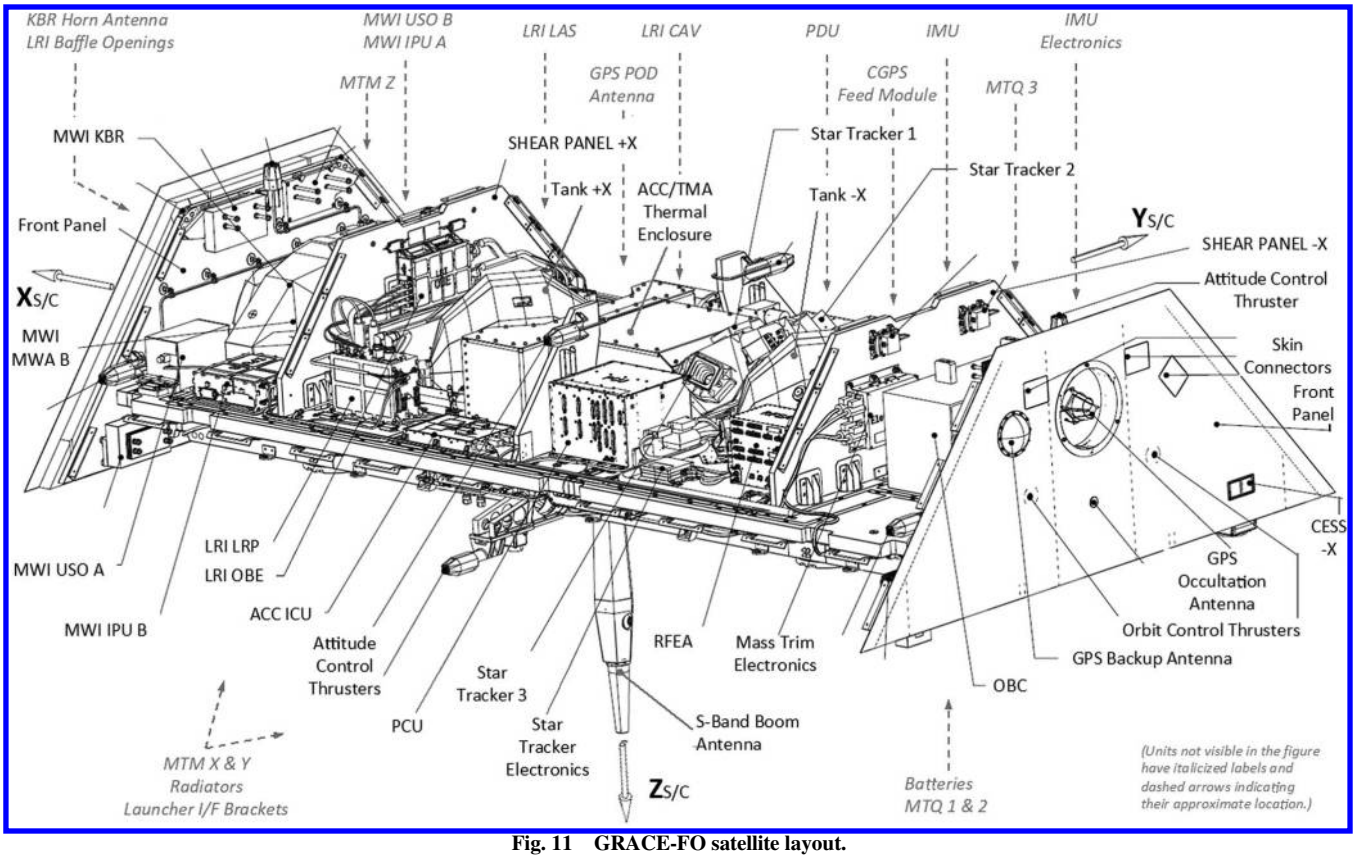

Fig. 11 GRACE-FO satellite layout.

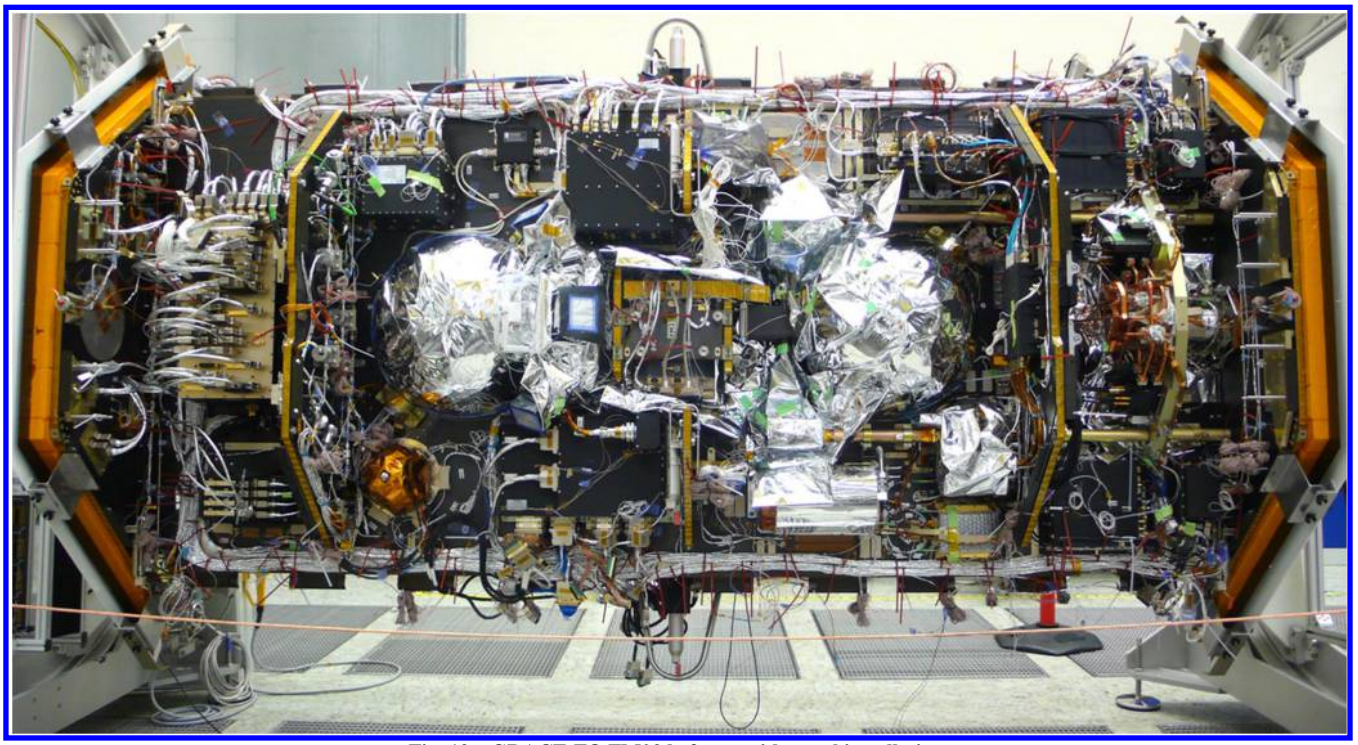

Fig. 12 GRACE-FO FM02 before zenith panel installation.

specific key requirements and the associated implementation to meet them for all the key subsystems. Figure 13 shows the overall GRACE-FO block diagram.

A. Spacecraft Structure and General Layout

Just as for GRACE, the two GRACE-FO spacecraft are designed to be identical in terms of form, fit, and function. The only differences between the two satellites are their spacecraft identification number and the radio frequencies used in the S-band transceivers and the MWI instruments. Both spacecraft can fly interchangeably in the leading or trailing positions, facing in the flight or antiflight direction, respectively. The GRACE structural design is maintained for GRACE-FO. It is based on a main equipment platform (MEP), trapezoidal front and rear panels with two trapezoidal shear walls in between, and three solar panels closing the trapezoidal structure box. At the bottom of the spacecraft, below the MEP and facing Earth, the spacecraft main radiator panel is mounted.

The majority of the spacecraft equipment and instrument units are mounted on the upper and lower sides of the MEP, with the rest mounted on the shear walls. The lower side of the MEP is reinforced by a stiffening framework, which also provides the interface to the four launcher interface brackets. The latter are different for GRACE-FO, as the spacecraft were launched on a SpaceX Falcon 9 launch vehicle, whereas the GRACE spacecraft were launched on a Russian Rockot launch vehicle. The MEP as well as all the panels are made out of sandwich panels comprising CFRP face sheets with an aluminum honeycomb core, providing high thermal and structural stability. The solar array panels and the front and rear panels have an additional layer of foam insulation on top of the outer CFRP face sheet.

The spacecraft spans 3.2 m in length (spacecraft X axis), 1.9 m in width (spacecraft Y axis), and 0.8 m in height (spacecraft Z axis), and has the same outer dimensions as GRACE. Because of the addition of the LRI and a number of improvements outlined next, the total wet spacecraft mass increased from 475 kg on GRACE to 600 kg on GRACE-FO. The overall packing density and ballistic coefficient are thus considerably increased compared to what they were for GRACE. The spacecraft mechanical layout is balanced to a priori minimize the distance between the spacecraft center of mass (CoM) and the ACC proof mass to minimize the coupling of spacecraft rotations into the ACC measurements. Moreover, to minimize disturbance torques caused by the residual atmosphere and the resulting thruster firings, the spacecraft are designed such that their in-flight center of drag is located along the longitudinal axis of the satellite originating at the CoM and coinciding with the geometric center of the MWI horn. Similarly, to minimize the relative movement between the spacecraft due to atmospheric disturbances, the ballistic coefficients of the two spacecraft have to be within 1.5% of one another.

B. Instrument Accommodation

The MWI accommodation on GRACE-FO is mostly unchanged from GRACE. The KBR support structure is mounted directly to MEP via three isostatic mounts. For GRACE-FO, the support structure has been modified to provide two holes to accommodate the LRI baffles. The USOs and IPUs are positioned onto the MEP to either side of the KBR structure; however, to balance the thermal load, the IPU and USO units from redundant strings are grouped together (e.g., A-side IPU with B-side USO).

The ACC accommodation on GRACE-FO has been adapted to cope with the tight mounting alignment requirements between the ACC and the TMA on one side, and ACC and the three star tracker heads (STR) on the other side. To this end, the ACC and TMA are mounted to a support structure box made up of four CFRP sandwich panels and referred to as the ACC/STR/TMA support structure (see Fig. 14). The ACC and TMA are thereby mounted to the same stiff CFRP baseplate, creating a dimensionally stable interface between the TMA and the ACC proof mass. Moreover, this all-CFRP-structure design provides homogenous material properties when subjected to thermal and/or moisture expansion, thereby keeping the TMA reference point coaligned with the ACC proof mass. The three star tracker heads are mounted to a silicon carbide "cube" (called SiC cube), providing both thermal and structural stability, and the SiC cube, in turn, is mounted to the other side of the ACC/STR/TMA support structure via three titanium isostatic mounts. The entire ACC/STR/TMA assembly is mounted onto the MEP via another three titanium isostatic mounts that form a circle whose center is coaligned with the ACC proof-mass location. Finally, to meet the stringent thermal stability requirements, discussed in the next section, the entire ACC/STR/TMA support structure, containing the ACC and TMA, is placed into a thermal enclosure.

All the LRI units are mounted to the MEP in the vicinity of the $+X$ shear wall except the optical bench electronics, which is mounted

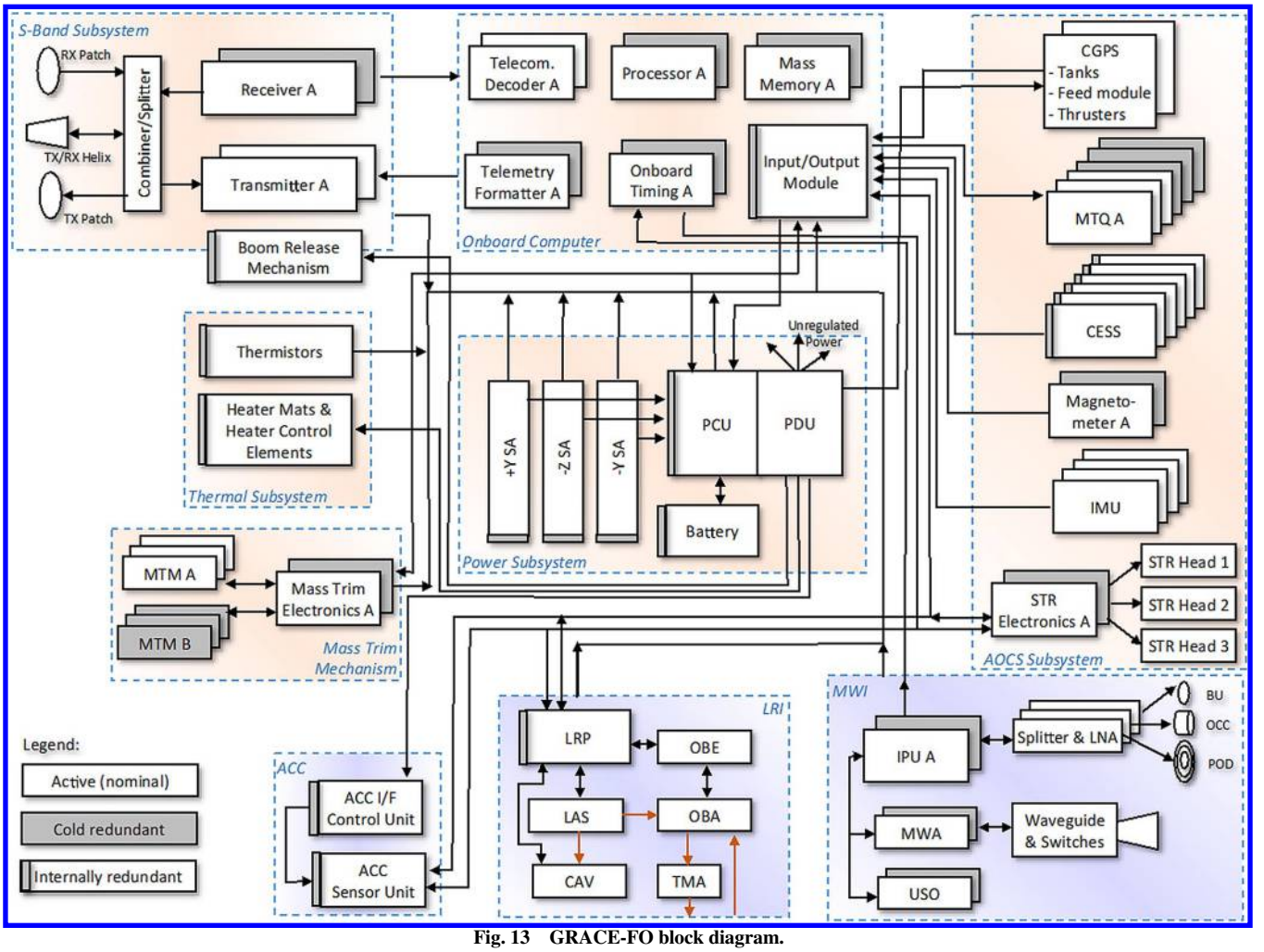

Fig. 13 GRACE-FO block diagram.

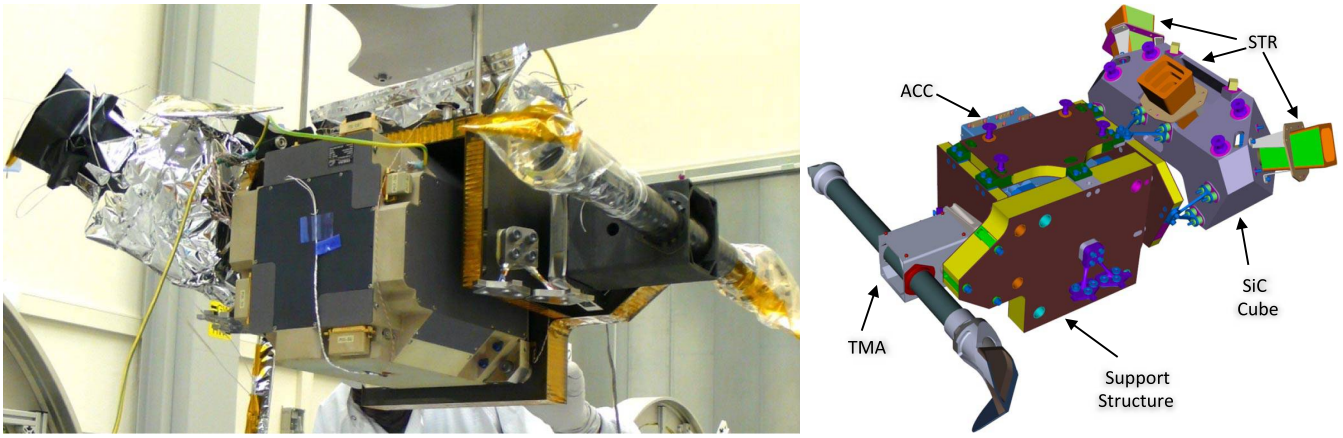

Fig. 14 ACC/STR/TMA assembly and SiC cube.

directly to the $+X$ shear wall. The baffle tubes, encapsulating the incoming and outgoing laser beams, are mounted to the MEP via dedicated support brackets and routed through holes in the $+X$ shear walls, KBR structure, and spacecraft front panel.

The thermal and mechanical aspects of the instrument accommodation are discussed in the next two sections.

C. Thermal Subsystem

The overall GRACE-FO thermal architecture follows the original GRACE thermal implementation but incorporates a number of improvements and lessons learned. The thermal design has to ensure that all allowable flight operating temperature ranges are met and maintained under nominal conditions. Furthermore, the design needs to be single-failure tolerant to guarantee that survival temperatures are maintained under off-nominal conditions. Finally, it has to provide the instruments with stringent temperature stability as well as, in the case of the LRI laser, accommodate a narrow absolute operating temperature range. Table 3 shows the driving thermal requirements for the instruments. The thermal stability requirements are expressed in terms of temperature variations per orbit (or multiple thereof), as the latter lead to thermoelastic distortions at orbital frequencies, which couple into the actual science measurement as

Table 3 Selected spacecraft requirements

	Spacecraft configuration	
Launch mass	Each spacecraft (fueled) $\leq$ 655 kg	
Ballistic coefficients	Difference < 1.5% between two satellites	
Center of drag (CoD)	CoD in $\pm X$-axis direction (with origin in the spacecraft CoM) with a tolerance of $\pm$5 mm	
	Thermal requirements	
ACC thermal stability	1) $\pm$0.1 K over one orbit period at temperature reference points (TRPs), with frequency content of the amplitude spectrum at 2/rev 0.04 K or less	
	2) $\pm$0.1 K/orbit at each interface point between spacecraft and ACC SU	
MWI and LRI thermal stability	Temperature stability per orbit:	
	USO: $\pm$0.40 K/orbit	TMA: $\pm$0.10 K/orbit
	IPU: $\pm$0.40 K/orbit	Laser: $\pm$0.10 K/orbit
	MWA: $\pm$0.24 K/orbit	OBA: $\pm$3.0 K/orbit
	Waveguide: $\pm$0.24 K/orbit	Cavity: $\pm$1.5 K/orbit
	Horn base: $\pm$0.40 K/orbit	OBE: $\pm$3.0 K/orbit
	24 GHz junction: $\pm$0.24 K/orbit	LRP: $\pm$3.0 K/orbit
LRI laser operating temperature	27–33°C	
	Ground alignments and alignment knowledge	
CoM relative to ACC fiducials	$\pm$550 μm in all three axes (translational alignment, including knowledge uncertainty)	
ACC fiducials relative to KBR structure fiducials	$\pm$500 μm in all three axes (translational alignment)	
	$\pm$3 mrad in pitch/yaw (rotational alignment)	
	$\pm$50 μm in all three axes (knowledge uncertainty)	
KBR Phase Center Offset Vector relative to ACC frame	$\pm$1 mrad (rotational alignment)	
	$\pm$0.2 mrad (knowledge uncertainty)	
Star tracker relative to ACC fiducials	$\pm$20 mrad in all three axes (rotational alignment)	
	$\pm$0.1 mrad in all three axes (knowledge uncertainty)	
TMA fiducials relative to ACC fiducials	$\pm$100 μm in Y, Z; $\pm$500 μm in X (translational alignment)	
	$\pm$0.25 mrad in all three axes (rotational alignment)	
	$\pm$12 μm in all three axes (knowledge uncertainty)	
	In-flight stabilities and center of mass migration	
ACC fiducials relative to CoM	1) $\pm$9 μm/orbit in all three axes (translational) with frequency content of the amplitude spectrum at 2/orbit less than 2 μm	
	2) $\pm$100 μm/6 months in all three axes (CoM migration)	
KBR relative to CoM (line-of-sight direction)	$\pm$11 μm/orbit in line of sight (translational) with frequency content of the amplitude spectrum at 2/orbit less than 2.5 μm	
Star tracker relative to ACC fiducials	$\pm$0.3 mrad in all three axes (rotational)	
TMA fiducials relative to ACC fiducials	$\pm$2 μm in X/orbit; $\pm$20 μm in Y, Z/orbit (translational)	
	$\pm$50 μrad/orbit in all three axes (rotational)	
	Attitude and orbit control requirements	
Intersatellite reference direction error	< 100 μrad for yaw and pitch (1-sigma) at a spacecraft separation of 170–270 km	
Pitch and yaw control power spectral density (PSD)	< 0.5 mrad/sqrt (Hz) over the frequency range of 0.0001–0.05 Hz	
Angular acceleration power spectral density (PSD)	Shall not exceed the following values:	
	Frequency range, mHz	Peak value [μrad/s^2/sqrt (Hz)]
	$> 5 - 500$	1.0
	0.2–5	$0.005/f$
Spacecraft providing pointing information to LRI	Spacecraft shall provide to LRI unit vector to the other spacecraft with an absolute knowledge error (AKE) of 400 μrad (3-sigma) and a relative knowledge error (RKE) of 230 μrad (3-sigma)	

tone errors. The requirements apply at predefined temperature reference points at the interface between the spacecraft and the instrument unit. The ACC sensor unit has the most stringent temperature stability requirement with $\pm$0.1 K over one orbit period, with the spectral content at twice per orbit bounded at 0.04 K. The second ACC sensor unit temperature stability requirement ensures that the gradient from a designated temperature reference point to any foot of the ACC is limited to $\pm$0.1 K over one orbit.

Similar to the ACC, the MWI unit stability requirements are needed to limit the temperature-induced errors in the one-way ranging measurement. The MWA, waveguides, and the 24 GHz junction have a stability requirement of $\pm$0.24 K/orbit. The GRACE-FO MWI stability requirements were adjusted from the ones levied onto the GRACE mission based on actual in-flight temperature measurements and updated error modeling. Among the LRI units, the TMA and the laser have the most stringent stability requirements with $\pm$0.1 K per orbit. Any temperature variations in the signal band for the TMA manifest themselves as path length changes, which could not be distinguished from the actual distance measurements and have therefore to be limited. Furthermore, for the laser to operate in a stable manner, the temperature stability requirement has to be met. The cavity, due to its large thermal mass and its passive temperature isolation design, requires a thermal stability of only $\pm$1.5 K/orbit. The LRI laser has, in addition to its tight thermal stability requirements, a very narrow operating temperature range of only 6°C, from 27 to 33°C, which the spacecraft has to maintain. Outside of this temperature range, the laser performance is expected to degrade.

The thermal design strategy relies on insulating the spacecraft's interior and providing moderate temperatures for all external environmental conditions. To achieve this, the satellite's primary structure is thermally insulated from space to the greatest extent possible. The solar array panels and the front and rear panels, composed of CFRP honeycomb sandwich panel, have a foam insulation layer on the space-exposed side of the panels. The outer surface of the foam, in turn, is covered by a CFRP face sheet with a Kapton or Kapton/silicon oxide (SiOx) foil on its external surface. For the solar array panels, the solar cells are glued directly onto the external Kapton foil.

Most of the equipment dissipating heat are mounted on the MEP, and to the extent possible, their respective mounting positions have been optimized for thermal aspects (in addition to mounting constraints, such as mass distribution and electrical configuration). The heat dissipated by the equipment is rejected via internal radiation and conduction to a main spacecraft radiator at the nadir side of the spacecraft. On GRACE, the nadir radiator foil moved due to Sun/eclipse exposure changes, causing mass movements that injected tone errors into the science data. To remedy this for GRACE-FO, the

Teflon/silver spacecraft radiator foil is attached to a set of eight rigid CFRP honeycomb panels, which cover the entire nadir side of the spacecraft and form a second enclosure below the MEP.

The spacecraft primary structure's thermal insulation is affected by a number of unavoidable heat leaks, including the launcher interfaces, thrusters, star trackers, S-band antennas, KBR horn, and GPS antennas. The spacecraft thermal design thus further includes an electrical heater system consisting of 72 independently controllable heaters to address cold orbit design cases and to allow for instrument temperature fine control. In an improvement over the GRACE design, the bang-bang heating control on GRACE was replaced with a linear heater control on GRACE-FO, thereby eliminating heater switching transients and associated range measurement tone errors, typical for bang-bang controllers. Each heater consists of a heater control element and an associated heater mat that are closed-loop controlled by the onboard computer. Redundant thermistors supply temperature measurements to the onboard flight software, which in a closed-loop fashion calculates the current to be supplied to the heater control elements. The heater lines are allocated in such a way as to provide full redundancy across the spacecraft (single-fault tolerant).

To meet the stringent ACC thermal stability requirement, a number of steps have been taken. The ACC sensor unit is mounted on an Invar sole plate (to increase its thermal capacitance) and conductively decoupled as much as possible from the spacecraft primary structure. The entire ACC/STR/TMA support structure, containing the ACC and TMA, is covered by a thermal enclosure, which is mounted to the MEP via thermal washers. The housing is thermally decoupled from the ACC/STR/TMA assembly and entirely covered by multilayer insulation (MLI) blankets. A dedicated internal radiator, consisting of an aluminum plate, is located in the spacecraft enclosure below the sensor unit, and radiatively transfers the heat from the ACC to the spacecraft radiator, serving as a damper of varying external heat fluxes.

The MWI K-band ranging system has stringent temperature requirements, but at the same time, the KBR has a high total heat dissipation that needs to be rejected to not overheat the components. To this end, the massive KBR structure panel serves as thermal mass to provide thermal stability. To thermally decouple it as much as possible from the thermal environment, the KBR panel is mounted to the MEP via three isostatic mounts using thermal washers and is completely enveloped by a closed MLI tent. Similar to the ACC, the KBR has a radiator mounted in the MEP compartment below it. The KBR dissipated heat is rejected to the KBR radiator conductively via flexible copper thermal links, from there radiatively to the spacecraft radiator. The already considerable thermal mass of the USO is further increased by a thermal interface plate, further improving the thermal stability, and its surface is enveloped in MLI.

Special consideration is given to the LRI laser, as it has both a very stringent thermal stability requirement as well as the narrowest operating temperature range of all the equipment on the spacecraft. Achieving these requirements is further exacerbated by the variability of the internal power dissipation, which depends on the heater settings controlling the laser frequency and the pump-diode operating temperature. To meet these challenges, the laser unit is mounted via four small interface feet to a massive thermal interface plate made of heat-conductive CFRP. The latter provides additional thermal mass, spreads the heat dissipated from the laser, and, due to matching coefficients of thermal expansion (CTEs), avoids thermal distortion of the MEP. The laser unit itself is gold-coated to minimize varying incident heat fluxes. While having internally stringent stability requirements, the cavity requires only moderate thermal stability at its interface to the MEP. Thermal stability is achieved via its large mass and massive titanium interface plate, as well as MLI blanketing. The OBA is mounted to the MEP via isostatic mounts, but provides its own passive thermal isolation and is wrapped with MLI. The LRI baffles encapsulate the laser beam from the TMA to the OBA and to the front panel of the spacecraft, where they have direct exposure to deep space and/or illumination by the Sun. To eliminate any thermal impacts on the interior, the baffles are wrapped in MLI and mounted on thermal washers.

D. Ground Alignments and In-Flight Stabilities

To meet the stringent range measurement requirements outlined in preceding sections, the spacecraft structure must meet a set of tight ground alignment, ground alignment knowledge, and in-flight stability requirements. Moreover, due to the addition of the LRI instrument and to ensure its coalignment with the MWI instrument, a number of additional alignment requirements have been added for GRACE-FO. The ground alignment, knowledge, and in-flight stability requirements are listed in Table 3.

The vector from the ACC proof mass to the KBR horn phase center defines the fundamental measurement vector for the range measurement and is referred to as the *KBR Phase Center Offset Vector*. It is this vector that has to be pointed to the other spacecraft, and its length has to be known and maintained once in orbit. The actual alignment is performed with respect to external fiducials on the ACC and the KBR structure, as only these are visible during mounting operations. The relative locations of the ACC proof mass and the KBR horn phase center with respect to their respective unit fiducials have been determined as part of unit-level metrology. As part of the ACC/STR/TMA assembly defined earlier, the star tracker measurement frame needs to be aligned with respect to the ACC measurement frame. Although the actual alignment is not as stringent, the *knowledge uncertainty* of the resulting alignment must be limited to ± 0.1 mrad, as it leads to both range and acceleration measurement errors.

With the addition of the LRI, a number of additional alignment requirements have to be satisfied. First, the TMA needs to be aligned both in position and in rotation, such that its vertex coincides with the ACC proof mass, as discussed previously. Next, to ensure coalignment between the MWI and LRI, the OBA needs to be positioned, such that the laser line is parallel to the vector from the ACC proof mass to the KBR phase center defined previously (rotational alignment), while intersecting the TMA mirror center (positional alignment). As for the ACC and KBR, the alignments are performed with respect to external fiducials, taking into account unit-level metrology relating the actual vertex to the fiducials. Additional alignments are specified for the LRI baffles to ensure that the LRI field of view is not obstructed.

Star tracker alignment knowledge was determined via a series of open-sky tests, as well as with an extensive camera calibration and metrology campaign. Alignments associated with the ACC/STR/TMA support structure were performed on a coordinate measurement machine, whereas measurements on the spacecraft were performed using a laser tracker. As all alignments are performed in an ambient pressure and temperature environment and under Earth gravity (1 g), the alignment budgets also need to account for a number of additional factors, to ensure that the alignments are maintained once the spacecraft reached orbit. To this end, the effects of outgassing and moisture release, and most important, the effects of the 1 g release, have been analyzed and incorporated into the error budgets.

Once in orbit, the spacecraft are subject to the thermomechanical distortions due to expansion and contractions during transition into and out of eclipse, as well as to center of mass migration over time due to differential fuel usage across both branches, addressed in the next section. The thermomechanical distortions occur at orbital rates (or multiple thereof) and couple directly into the science measurements; for example, the distance between the KBR horn phase center and the ACC proof mass has to be kept constant, as variations in the distance between them cannot be distinguished from actual changes in the distance between the two spacecraft. Similarly, the center of mass, the star-tracker-to-ACC, and the TMA-to-ACC alignments vary as a function of the thermomechanical distortions the spacecraft experiences in orbit. To mitigate these thermomechanical distortions, significant use of CFRP in the primary and secondary spacecraft structures has been made to stiffen the overall spacecraft structure, as discussed in previous sections. Furthermore, to verify that the resulting spacecraft structure meets all the requirements stated previously, a distortion analysis covering worst-case hot and cold orbits has been conducted.

E. Center-of-Mass Control and Mass Trim Mechanisms

To measure the acceleration of the spacecraft center of mass (CoM) with the greatest possible accuracy, the ACC proof mass needs to be positioned and maintained as closely as possible to the spacecraft CoM. Because the ACC's location can no longer be adjusted once the ACC is mounted in the ACC/STR/TMA assembly and the latter structure integrated into the spacecraft, it is the CoM location that needs to be managed and maintained through the assembly of the spacecraft and in the course of the mission. To this end, a number of requirements for CoM control are levied onto the spacecraft implementation, as shown in Table 3.

During assembly of the spacecraft, the spacecraft CoM has to be controlled to less than 550 μm from the position of the ACC proof mass in all three spacecraft axes. The requirement includes an allocation for a CoM shift at the time of launch and insertion into orbit due to 1 g gravity release (i.e., the transition from 1 g to 0 g), as well as subsequent moisture release by the CFRP and the insulation foam over the course of the initial mission. Once the spacecraft are in orbit, the CoM offset has to be further reduced to within 100 μm of the ACC proof mass for initial science operations [25]. Moreover, as small differences in fuel usage and leakages across both thruster branches will lead to CoM migration over time, the CoM offset to the ACC proof mass has to be regularly maintained throughout the mission. Similar to GRACE, the CoM migration is required to stay within 100 μm over the course of a six month period. To compensate the effects of the initial CoM offset at launch and the postlaunch CoM migration, movable mass trim mechanisms (MTMs) in all three spacecraft axes had to be added to the spacecraft design. In-orbit CoM calibration maneuvers have then to be performed and the MTMs adjusted accordingly, as explained next in more detail. Finally, the MTMs are required to offer at least 10% margin for the expected CoM migration over the life of the five year mission.

The process of CoM control, and mass properties in general, starts during the layout of equipment onto the MEP. Through careful positioning of the units, the need for balance masses is minimized. For this purpose, the two propellant tanks are positioned symmetrically on each side of the expected CoM location. The final prelaunch mass properties requirements are verified by performing a mass-balancing spin test, and where needed, non-movable balance masses are installed on eight brackets that are mounted on the $+X$ and $-X$ panels (four on each panel) to meet the tight 550 μm CoM requirement.

The MTM, used for in-orbit trimming, consists of a cuboid trim mass that is movable in one axis by a worm roller screw. The latter is connected to a stepper motor through a planetary gear box. The trim mass weighs approximately 5.5 kg and is made of a nonmagnetic alloy. The trim-mass stepper motor is commanded in an open-loop fashion via ground commands, but operations are facilitated by the availability of limit switches at the approximate center of travel and by mechanical end stops at the end of the travel range.

The GRACE MTM design has been adapted slightly for use on GRACE-FO to provide an increased trim range. This was required due to GRACE-FO's larger spacecraft mass and the consideration of additional in-flight CoM motion effects observed on GRACE. As for GRACE, two MTMs are mounted along each spacecraft axis providing a spacecraft CoM trim capability of at least ± 1.9 mm in the X axis, and ± 1.5 mm in the Y and Z axes, respectively, for a maximum allowable satellite mass of 655 kg. Within this range, a spacecraft CoM displacement step size as small as ± 0.01 mm can be achieved.

During launch, the MTMs are positioned in their centered position. Once in orbit, a dedicated calibration maneuver is performed to establish the actual CoM offset relative to the ACC proof mass. The calibration maneuver is conducted by alternating every 6 s between the maximum positive and negative commanded magnetorquer commands for a total maneuver duration of 180 s. The maneuver is repeated in different spacecraft axes and at different orbit positions, and results in a defined spacecraft rotation around the CoM in each axis. By analyzing the corresponding ACC measurement data, the offset between the ACC proof mass and the spacecraft CoM can be evaluated and the MTMs commanded to correct for this offset. See Ref. [25] for more detail on the CoM calibrations done for the GRACE mission.

F. Attitude and Orbit Control Subsystem

The GRACE-FO Attitude and Orbit Control System (AOCS) is responsible to provide attitude knowledge and control, as well as orbital control and maintenance throughout all mission phases while satisfying all GRACE-FO mission requirements. The key AOCS requirements are listed in Table 3. After launch and launch vehicle separation, the AOCS damps residual spacecraft turn rates introduced at separation, acquires coarse and subsequently fine attitude knowledge, and establishes a nadir-pointing attitude. Based on ground commanded maneuvers, proper orbital separation at 220 ± 50 km distance is established using the orbital control thrusters. Once the spacecraft and instruments are fully commissioned, the AOCSs on both spacecraft establish fine pointing control to ensure the instrument boresights on both spacecraft are pointed at each other. To this end, the knowledge of both spacecraft's position is uploaded via Two-Line Elements (TLEs) to both satellites by the ground teams and propagated via onboard orbital propagators. The relative pointing vector is established by differencing the propagated position of both spacecraft and computing the local horizontal plane from the spacecraft's own GPS solution.

The error in the reference pointing direction computed onboard for the intersatellite K-/Ka-band reference pointing direction has thereby to be less than 100 μrad (1-sigma) for yaw and pitch at a spacecraft distance between 170 km and 270 km. Two additional requirements are levied on the attitude control system performance in the form of power spectral densities. First, to limit multipath and related antenna offset errors coupling into the science measurements, the power spectral density (PSD) of the pitch and yaw variations relative to the commanded attitude has to be limited in the frequency range relevant for science. Second, to limit accelerometer observations being corrupted by its residual offset from the CoM, the PSD of the spacecraft angular acceleration has to be constrained, as shown in Table 3. Finally, with the addition of LRI, the AOCS needs to provide the LRI instrument with additional reference direction information, roll angle, as well as range rate relative to the other spacecraft, to allow the LRI to point its mirror to the other spacecraft, as the fluctuations in the spacecraft pointing (dead-banding) are larger than the beam convergence of the outgoing beam. In addition, the AOCS has to support K/Ka-band and CoM calibration maneuvers, as explained in subsequent sections.

The GRACE-FO AOCS has been designed for a gravity-field mission, incorporating a number of improvements over the original GRACE mission. The AOCS design enables three-axis stabilized (Earth) pointing at all times. The compact satellite design based on a long slender spacecraft body with body-fixed solar arrays minimizes the external disturbance torques and enables an AOCS actuator concept relying on magnetic torque rods supplemented by a low-thrust cold-gas propulsion system. The AOCS sensor suite has been augmented compared to the set flown on GRACE, and includes a suite of star tracker heads, a high-performance inertial measurement unit (IMU), redundant fluxgate magnetometers, and a set of six coarse Earth–Sun sensors (CESSs). The AOCS sensor information is further augmented by GPS position and velocity information provided by the MWI GPS receiver.

The number of star tracker heads has been increased from two to three based on a lesson learned from GRACE, where blinding of one star tracker head by the Sun or Moon left the attitude control system temporarily with one head only. The three star tracker heads are mounted on the ultrastable SiC cube that is attached to the ACC/STR/TMA support structure described previously. Their boresights are aligned to optimize sky coverage, and they are mounted with a separation angle large enough to ensure that simultaneous blinding of more than one star tracker head by the Sun, Earth, or Moon is minimized to a small fraction of the time during the mission. Moreover, because the star tracker head performance around its boresight axis is about 10 times worse than about its two lateral axes,

the availability of multiple star tracker head measurements allows for a better performance about all axes by fusing attitude information from multiple heads. The three heads are cross-strapped to redundant star tracker electronics, which interface with the onboard computer.

In a further improvement over GRACE, the single three-axis coarse-performance IMU was replaced by a four-axis high-performance fiber-optic IMU. In addition to increased performance, the arrangement of the four angular rate sensors in a skewed configuration provides a single-failure redundancy. Unlike other technologies, such as ring-laser or mechanically tuned gyros that employ dither mechanism, the fiber-optic technology is also well suited for GRACE-FO, as it avoids generating microvibrations. The IMU measurements are used as a direct rate measurement for the derivative part of the controller, as well as to propagate spacecraft attitude between star tracker measurements. Two redundant three-axis fluxgate magnetometers, compared to just a single fluxgate magnetometer sensor head on GRACE, are used for magnetorquer control during acquisition and safe mode, and as a backup rate sensor in case of an IMU failure. The fluxgate magnetometers are mounted on the front panel, sufficiently far away from the magnetorquers to minimize the effects of induced fields generated by the latter units.

A set of six coarse Earth–Sun sensors provides reliable and robust attitude measurements of the Sun and Earth vectors in the spacecraft coordinate frame. The sensor heads are installed on each side of the spacecraft, pointing along the positive and negative directions of all three spacecraft axes, thereby providing omnidirectional coverage, and enabling initial acquisition and coarse pointing mode without performing active search maneuvers. The sensor is also used for monitoring during normal operation to detect coarse attitude deviations. Each sensor head consists of multiple redundant thermistors sensing the irradiated flux from the Sun and Earth using different filters. With this information, the AOCS flight software is able to determine the Sun and Earth vectors in the spacecraft frame. Finally, two redundant GPS receivers, part of the MWI IPU, provide position, velocity, and time measurements to the AOCS. The information is used to propagate the spacecraft orbit position and establish the local-vertical/local-horizontal frame.

The actuator suite consists of three redundant magnetorquers (MTQ) as the main actuator for compensating environmental disturbance torques, and they are supplemented by a redundant cold-gas propulsion system (CGPS) for orbit maintenance and attitude slew maneuvers, and to provide control authority in excess of what the magnetorquers are capable of. Each magnetorquer consists of redundant wounded coils around a high-permeability core material and provides a magnetic dipole moment of ± 27.5 Am, sufficient for counteracting environmental disturbances most of the time. The three magnetorquers are mounted orthogonally to each other, one aligned with each spacecraft axis. They are accommodated on the spacecraft side that is furthest from the MWI instrument (i.e., on the $-X$ side of the spacecraft) to minimize the induced field generated by the torquers on the MWI and magnetometers.

The cold-gas propulsion system is using gaseous nitrogen (GN2) and consists of 12 attitude control thrusters and two orbit control thrusters, arranged in two branches with six attitude control thrusters and one orbit control thruster each. The attitude control thrusters provide 10 mN thrust with a specific impulse (I_{SP}) of more than 70 s and are used for attitude control in excess of the capability of the magnetorquers, for example, for slews to and from burn attitudes. They are arranged to provide force-free attitude control (no net ΔV) by firing a pair of thrusters, one on each branch, which are facing in opposite directions. However, because even in a force-free thruster arrangement there is ultimately a residual impulsive linear momentum (and an associated velocity change) when a thruster pair is fired, the roll and yaw attitude control thrusters are oriented in the out-of-plane direction (cross-track) to minimize any impact on in-plane accelerometer measurements. The pitch control thrusters are pointed in the radial direction, but as for GRACE, it is expected that they are infrequently actuated due to sufficient control authority of the pitch magnetorquer in a near-polar orbit [12]. The orbit control thrusters provide 50 mN each, compared to the 40 mN thrusters used on GRACE, with the latter not available anymore. They are mounted on the spacecraft $-X$ end panel and are canted to point through the spacecraft CoM. They can be fired individually or as a pair, in which case a net force of 78 mN along the X axis is obtained, and they are used for constellation establishment and maintenance maneuvers. Attitude and orbit control thrusters are nearly identical, whereby the different thrust levels are achieved with different throat diameters, respectively.

To satisfy the mission ΔV requirements with ample margin, each spacecraft carries approximately 31 kg of GN2, providing a ΔV capability of more than 34 m/s. The GN2 is stored in two identical composite-overwrapped 52 L tanks with an expected maximum operating pressure of 310 bar. The two tanks are arranged on both sides of the spacecraft CoM and attached to one of the thruster branches each. In between the two tanks, a nominally closed high-pressure solenoid valve is installed to limit the mass flow between them due to thermal gradients. To ensure concurrent depletion of both tanks and maintain tight CoM control, both thruster branches are operated simultaneously. With its two branches, the propulsion system is dual redundant, as the mission objectives can be achieved with a single branch only (albeit no longer with force-free attitude control). Additional redundancy is obtained via a series of latch valves in both the high- and low-pressure segments of the propulsion system, allowing the isolation of a propulsion system element.

The AOCS control loop, including the commanding of magnetorquers and thrusters, is executed at 2 Hz. Star tracker measurements and IMU data are acquired at 2 and 8 Hz, respectively, whereas fluxgate measurements and coarse Earth–Sun sensor data are available at 1 Hz, and GPS position and velocity data at 0.5 Hz. In addition to controlling the boresight to the other spacecraft, additional pointing reference information, that is, the vector to the distant spacecraft, is also provided to the LRI at 2 Hz to aid in the initial acquisition before implementing closed-loop wavefront sensing and control.

Upon commissioning the MWI instrument, and when needed throughout the mission, the spacecraft performs a series of calibration maneuvers to locate the phase center in the MWI horn. Should the phase center be offset from the geometric center of the horn, the spacecraft pointing attitude can be offset to point the horn phase center toward the other spacecraft.

G. Power Subsystem

The power subsystem is responsible for the generation, conversion, regulation, and distribution of primary power to all the bus units and instruments onboard GRACE-FO. It consists of three solar array panels for power generation, a lithium ion battery for energy storage, and a power conversion and distribution unit, responsible for power conversion, regulation, and distribution.

The power subsystem architecture for GRACE-FO was modified in a number of areas compared to GRACE. The accommodation of the LRI resulted in an increased power demand on the power subsystem. At the same time, the addition of the third star tracker head and the additional cutout in the zenith-facing solar panel resulted in the reduction of solar panel area. Furthermore, the adoption of linear heater control, instead of the bang-bang heater strategy used for GRACE, avoids the thermal disturbances seen on GRACE during heater switching, but levied additional functionality on the power distribution electronics.

The three body-fixed solar array (SA) panels are part of the spacecraft trapezoidal structure box with the two side panels tilted toward the $+Y$ and $-Y$ directions, and the top panel oriented in the $-Z$ direction, respectively (see Fig. 15). To accommodate the increased power demand and reduced solar array area, state-of-the-art triple junction gallium arsenide (GaAs) solar cells were chosen with an advertised efficiency of 28%. The cells were originally qualified for the Swarm mission but were subjected to an additional delta-qualification program for GRACE-FO to account for the different temperature cycles and lifetime requirements. The use of GaAs resulted in a significant power increase compared to the power output of the silicon cells used on GRACE. The top panel is expected to provide in excess of 350 W, whereas each of the two side panels is

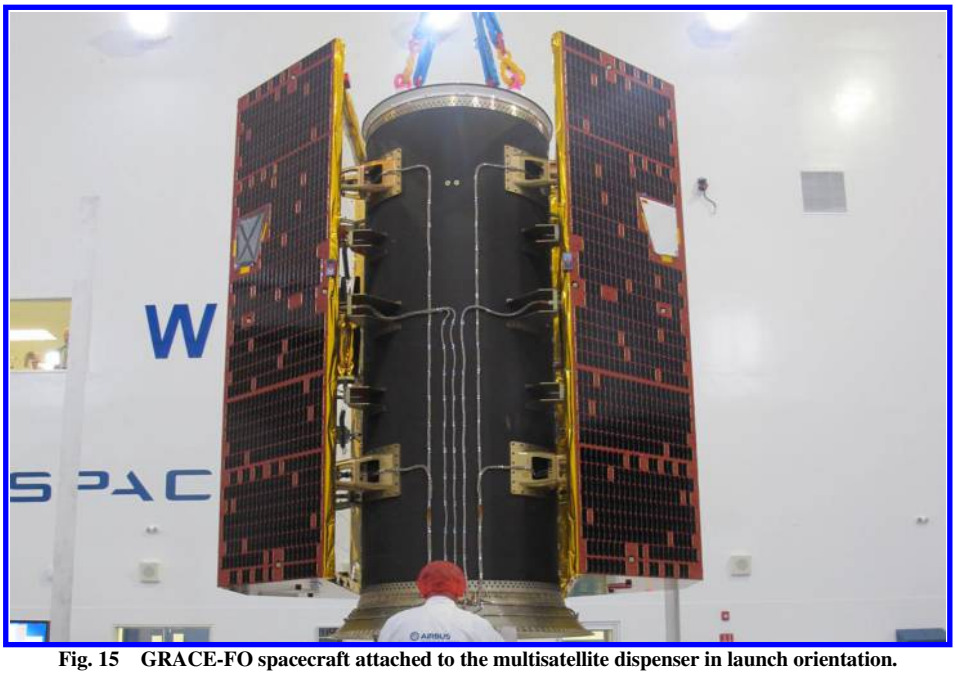

Fig. 15 GRACE-FO spacecraft attached to the multisatellite dispenser in launch orientation.

capable of generating more than 510 W under worst-case and end-of-life conditions.

To accommodate a higher power draw during eclipse and provide additional power margin, a 78 Ah lithium-ion battery is baselined, which provides a significantly better specific weight and volume to energy ratio than the nickel–hydrogen battery type used on GRACE. The battery was sized to satisfy the launch energy budget, requiring enough capacity to supply the spacecraft from launch to initial acquisition under off-nominal conditions. A battery passivation function was added to allow the depletion of the remaining battery energy at the end of the mission.

The power conversion and distribution unit (PCDU) is based on a similar unit used on the Swarm mission, but it was split into a power conversion unit (PCU) and power distribution unit (PDU) for GRACE-FO to facilitate the mechanical accommodation on the spacecraft structure. The power conversion unit contains a maximum power point tracker to optimize power production, autonomous battery (charge/discharge) management, and autonomous power fault management. The power distribution unit provides unregulated main bus power to all bus units and instruments via latching current limiters, and it contains the propulsion drive circuits for the latch valves, solenoid valves and thrusters, the power and control signals for 72 heater circuits, and the S-band boom release activation circuits. In addition, the power distribution unit provides a secondary power bus in the form of a regulated 28 V bus to the ACC interface control unit.

H. Onboard Computer and Flight Software

The onboard computer (OBC) is at the center of the GRACE-FO command and data handling system. The OBC is an internally redundant computing platform based on the ERC32 radiation-tolerant single-chip microprocessor, and has flight heritage (e.g., on Swarm, GOCE, and CryoSat-2) with no adaptions for GRACE-FO. It hosts the onboard flight software functions responsible for onboard data handling and storage, AOCS, thermal control system, fault detection, isolation and reconfiguration, and timing data and synchronization signal generation and distribution.

The OBC contains, in one physical box, 1) fully redundant processor modules, 2) telemetry and solid-state mass memory units, providing data storage of 12 Gbit for science data and 4 Gbit for housekeeping data, 3) telecommand modules, supporting downlink data rates of 31.25 kbit/s and 3 Mbit/s, and uplink rates of 4 kbit/s, 4) reconfiguration modules, storing critical spacecraft parameters and recovery sequences, and providing spacecraft timing services, and 5) power supplies. In contrast, the GRACE spacecraft supported a high-rate downlink of 1 Mbit/s only.

Command, control, and data transfer between the OBC and the GRACE-FO instruments and star trackers are implemented via asynchronous serial point-to-point (universal asynchronous receiver transmitter, or UART) interfaces, whereas synchronous serial digital interfaces are used for communications with the power distribution unit and mass trim electronics. In addition, a Mil-Standard 1553B bus is implemented for data exchange with the IMU, as well as for communications between the OBC's main elements. Finally, a number of discrete digital and analog input/output interfaces are used to interface with the thermistors, relays, fluxgate magnetometers, magnetorquers, as well as cold-gas propulsion system telemetry.

One of the key functions of the OBC is the distribution of timing information to the instruments and the star tracker in the form of a pulse-per-second signal (PPS) and an accompanying time packet advertising the spacecraft time corresponding to the leading edge of the PPS. This allows the science team to correlate all measurements to a common time basis. To this end, the OBC can operate in one of two possible modes, either in externally synchronized mode or in free-running mode. In its nominal mode, the OBC is synchronized to the stable PPS signal supplied to it by the MWI IPU. The OBC locks onto this signal to maintain its onboard reference time, and then redistributes the signal to the instruments and the star trackers. As a lesson learned from the GRACE mission, the free-running mode capability was added to the OBC, allowing it to propagate the PPS signal based on its OBC internal clock source, albeit at reduced accuracy, in case of intermittent outages of the externally supplied MWI PPS.

The GRACE-FO onboard flight software design is based on the deterministic execution of activities by relying on a table–driven approach with static scheduling that was already employed on Swarm and GRACE. This allows the reuse of a significant amount of Swarm flight software for GRACE-FO for functions, such as data handling. However, due to the mission-specific implementation of AOCS and thermal control for GRACE-FO, the associated flight software functions and modules had to be developed, coded, and tested specifically for GRACE-FO.

As part of the GRACE-FO's command and data handling, the OBC will collect instrument and bus unit telemetry, store it in its mass memory unit, and downlink during overflights; similarly, telecommands received will be decoded, validated, and routed to the appropriate recipients. To accomplish this, the GRACE-FO mission

adopted the GRACE-FO Packet Utilization Standard, which was derived from the European Cooperation for Space Standardization (ECSS) Telemetry and Telecommand Packet Utilization Standard and was used on Swarm as well.

The Fault Detection, Isolation, and Recovery (FDIR) approach is derived from the Swarm FDIR design, and provides the spacecraft the capability to detect and recover from single failures either at the unit or system level. Although a recovery from multiple concurrent faults is not required, spacecraft fail-safe conditions can be established in many multiple-fault failure scenarios. This resiliency is achieved by implementing a multitiered FDIR approach, covering unit-level FDIR, instrument- and subsystem-level FDIR, spacecraft-level FDIR performed by the OBC flight software, and spacecraft-level FDIR performed by hardware monitoring.

I. Telecom Subsystem

The communication subsystem receives telecommands from the ground station and relays them to the OBC for execution, as well as routes telemetry and science data from the satellites to the ground station. It operates in the S-band at the frequencies of the original GRACE mission. Each spacecraft will have distinct uplink/downlink frequencies, which, in addition to the different K/Ka-band frequencies of the MWI instrument, constitute the only nominal differences between the two spacecraft.

The S-band communication consists of an internally redundant RF Electronics Assembly (RFEA), a helix transmit/receive antenna mounted on a deployable boom on the nadir side of the spacecraft, and two patch antennas, one transmit and one receive, mounted on the spacecraft zenith panel. The nadir boom-mounted antenna will deploy via a spring mechanism shortly after launch vehicle separation, and serves as the prime transmit/receive antenna throughout nominal mission operations, whereas the zenith-facing patch antennas serve as backup antennas in case the spacecraft experiences off-nominal attitude conditions. The S-band subsystem supports the two downlink data rates of 31.25 kbit/s (low-rate mode) and 3 Mbit/s (high-rate mode), and an uplink rate of 4 kbit/s via both helix and receive patch antennas. The length of the boom is approximately 0.7 m, and it serves to limit any signal reflections on the spacecraft structure as well as to maximize the helix antenna pattern coverage.

The RFEA contains two hot-redundant receivers, two cold-redundant transmitters, and two signal combiners/splitters, all in a single chassis. The original GRACE S-band transceiver was no longer available due to part obsolescence, and the GRACE-FO RFEA constitutes thus a new development, bringing the old GRACE analog design to an all-digital implementation. Signals received via the nadir and zenith antennas are (constructively) combined and routed to the two hot-redundant receivers, where they are binary phase-shift keying (BPSK) demodulated and routed to the command decoders of the OBC. Because both receivers are powered, the first one declaring an RF- and data-valid flag is designated by the OBC as the prime receiver. Telemetry data, consisting of spacecraft housekeeping and science data, received from the OBC encoder are offset quadrature phase-shift keying (OQPSK) modulated in the prime transmitter, and then routed to both the nadir-facing helix and zenith-facing patch antennas for transmission. The prime transmitter is turned on by the OBC via a ground-sequenced mission timeline ahead of an expected ground station overflight, whereas the backup transmitter is nominally powered off, but can be activated if the prime transmitter fails.

V. Launch and Operations

A. Launch and Early Operations

Unlike the GRACE mission, which launched on a Russian Rockot launch vehicle from Plesetsk Cosmodrome in Russia, GRACE-FO launched onboard a SpaceX Falcon 9 launch vehicle from Vandenberg Air Force Base, California, on 22 May 2018. During the launch, both spacecraft were mounted on the sides of a multisatellite dispenser (Fig. 15). As for the GRACE mission, a polar orbit with an altitude of 490 km, an inclination of 89 deg, and eccentricity less than 0.005 was targeted. Once the proper orbit was reached, the satellites were released from the multisatellite dispenser. The use of push-off springs ensured a relative velocity being imparted on the two spacecraft, which set them on separating trajectories.

On each satellite, the separation event was detected via separation straps, and initiated a series of autonomous spacecraft reconfigurations to establish a power-safe, thermally stable, and commandable attitude. The spacecraft angular tip-off rates imparted at separation were damped and a coarse Earth-facing attitude was established using the coarse Earth-Sun sensor measurements. Within 60 s after separation, the S-band antenna boom was released and the RFEA started transmitting low-rate telemetry.

In the course of the first ground station overflights, the telemetry rate was adjusted to high rate. The MWI USO and IPU were turned on to obtain onboard GPS solutions and synchronize the OBC real-time clock to the IPU-provided timing information. With the availability of star tracker data, the spacecraft was commanded to transition from its postlaunch safe mode into a nominal nadir-pointing attitude (i.e., the spacecraft radiators nadir pointed and the spacecraft longitudinal axis pointing along the velocity vector). Once the nominal separation distance of 220 ± 50 km between the satellites had been achieved in the first few days after launch, a separation arrest maneuver was performed, which reduced the relative velocity between the two spacecraft to less than ± 3 m/s.

Over the course of the first few months, the spacecraft bus units and instruments are checked out, calibrated, and commissioned for science. With the upload of TLEs to both spacecraft, satellite fine-pointing was enabled and the two spacecraft slewed to point the MWI horn antenna to each other. Both ACC and MWI were then turned on, and after a performance checkout transitioned into science mode on both spacecraft. A CoM calibration maneuver was performed and the MTMs adjusted, where needed, to reduce the offset between the CoM and the ACC proof mass to less than 100 μm, as discussed in preceding paragraphs. The LRI was turned on and performed extensive checkout activities on each spacecraft individually, before successfully establishing the intersatellite link between both spacecraft. In the first year, the LRI is operated in parallel with the MWI for at least three months to evaluate its ranging performance. If needed, a KBR boresight calibration maneuver is conducted to establish the effective KBR boresight and bias the pointing attitude accordingly.

Figure 16 shows an initial in-orbit demonstration of the MWI's performance. It depicts a single ground track of the GRACE-FO observatory (top), Earth's topography along the ground track (bottom), and the corresponding changes in distance between the two spacecraft as measured by the MWI (middle), after the gross relative motion due to the differences in their orbital initial conditions has been removed. With the topography and mass distribution underneath the observatory changing (e.g., during overflight over mountain ranges), the change in intersatellite distance measured by the MWI is clearly discernable and in good agreement with expectations. For the ground track shown, the observed changes in intersatellite distance are largest over the Himalayas with distance changes larger than 100 μm, and the figure is thus informally referred to as "the Himalaya plot." A similar initial performance demonstration of the LRI was performed two weeks later, and initial results are discussed in Ref. [26].

B. Science Operations

The GRACE-FO mission is operated from the DLR's German Space Operations Center (GSOC) in Oberpfaffenhofen, Germany, using the DLR ground stations in Neustrelitz and Weilheim, Germany, for uplink and downlink, and GFZ's satellite receiving station in Ny-Ålesund on Spitzbergen as an additional downlink venue (as well as backup uplink channel). In addition, NASA's Near Earth Network provides its ground stations for uplink/downlink in early operations and in contingencies.

During routine science operations, up to 3.7 Gbit/day of instruments and spacecraft data for each satellite are expected to be downlinked and disseminated to the science teams located at JPL, GFZ, and the University of Texas Center for Space Research

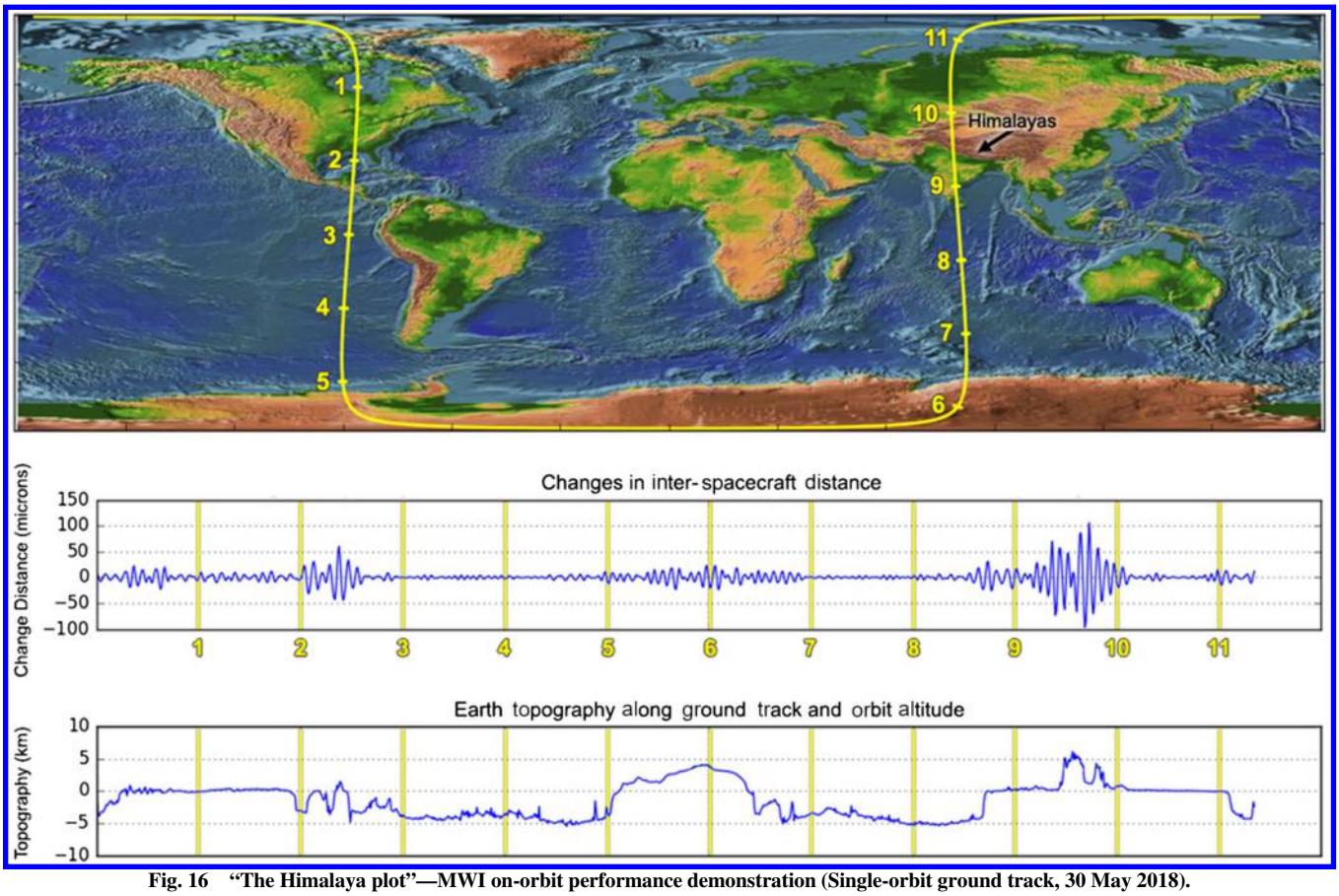

Fig. 16 "The Himalaya plot"—MWI on-orbit performance demonstration (Single-orbit ground track, 30 May 2018).

(UTCSR), in Austin, Texas. Instrument measurements accumulated over a 30 day period are processed by the latter teams to generate a global gravity field once a month. Moreover, 200 radio occultation measurement profiles of Earth's atmosphere, obtained by the MWI via its radio occultation antenna, are acquired and downlinked daily, supporting weather forecasting.

Each spacecraft's knowledge of its own and the other satellite's ephemeris has to be maintained to ensure that both spacecraft continue to point at each other. To this end, orbit determination using the downlinked GPS measurements of both spacecraft is performed by GSOC, and the resulting TLEs for the ephemeris of both spacecraft are uplinked to each satellite on a daily basis. Although the uploaded TLEs are sufficient to keep the MWI pointed at each other, the LRI acquisition has to be further aided by uploading a set of parametric corrections to the LRI that are based on high-precision orbit determination from downlinked GPS data [27].

C. Orbit Maintenance and Decommissioning

Once launched into their initial orbits, the spacecraft orbits are decaying freely. It is expected that, at the end of the primary mission, the spacecraft orbital altitude will have decayed to approximately 450 km. However, throughout the mission, their relative distance has to be kept to within 170–270 km (approximately 2 deg separation). To keep pointing at each other, the leading and trailing satellites are pitched up and down by approximately 1 deg relative to the velocity vector, respectively, leading to differential drag acceleration and changing distances between the two spacecraft. Station-keeping maneuvers are thus performed to keep them within their nominal separation range.

With atomic oxygen present in the rarefied atmosphere, the spacecraft and instrument surfaces, such as the KBR horn antenna, may be exposed to the effects of atomic oxygen erosion over time, although the exposure is greater for the spacecraft side pointed in the ram direction. In addition to using erosion-resistant materials and SiOx coatings for additional protection, two spacecraft position interchange maneuvers are planned throughout the mission to switch the positions of the leading and trailing satellites, and thereby ensure uniform exposure across both spacecraft.

At the end of the GRACE-FO science phase, the GRACE-FO satellites are decommissioned. The two spacecraft perform cold-gas propellant depletion maneuvers to place them on nonintersecting trajectories and eliminate any risk of collision. Built-in battery passivation switches are opened to prevent the batteries from being charged and deplete the remaining charges. With the bus voltage steadily declining, the spacecraft cease to operate, and due to orbital decay, ultimately disintegrate during atmospheric entry.

VI. Conclusions

This paper surveyed the GRACE-FO mission, conceived to succeed the recently decommissioned GRACE mission and, at the same time, demonstrate the first-ever in-space intersatellite laser ranging interferometer as a technology pathfinder for future gravity mapping missions. The science requirements, the mission concept, and the measurement error sources were discussed, and the instrument suite, consisting of the Microwave Instrument, the accelerometer and the newly added laser ranging interferometer, was reviewed. The satellite design implementation and the requirements that drove it were then examined. Finally, the approach to operations was briefly touched on.

Although the starting point of the GRACE-FO spacecraft development was footed in the original GRACE spacecraft for a number of aspects, including the mechanical, propulsion, and thermal design, it distinguished itself in significant ways from the latter. The command and data handling, as well as the power and sensor suite, were based on the Swarm spacecraft. Next, significant changes to the overall spacecraft layout as well as increased complexity compared to the original GRACE design were incurred due to the accommodation of the LRI. Finally, a number of additional improvements were incorporated based on lessons learned from both the GRACE and Swarm missions, leading to an overall more robust

implementation. Areas of particular attention during the design and implementation included structural alignments and in-flight stability, thermal stability control, center of mass control throughout the design and in flight, and attitude and pointing control.

Whereas the latter aspects of the instrument and spacecraft design are crucial to a gravity mapping observatory and have been successfully addressed, the GRACE-FO and future gravity missions still have to contend with measurement limitations due to instrument measurement noise, as well as the limited temporal and spatial sampling frequency of a single gravity observatory, that is, its inability to measure changes in the gravity field, such as tides, that occur faster than they can be observed. The GRACE-FO in-orbit demonstration of the LRI is a milestone in enabling future instruments with lower instrument noise, while future gravity missions may employ multiple satellite pairs at the same time to provide increased spatial and temporal resolutions.

Designing and implementing the GRACE-FO mission was a complex endeavor involving the close collaboration of multiple organizations across the United States, Germany, and France, and the successful project execution is a testament to the successful partnership between all involved teams. With its launch in May of 2018, the GRACE-FO observatory continues the successful legacy of its predecessor, but also leads the way in demonstrating the first-ever in-space intersatellite laser ranging interferometer. As future geodesy missions with similar challenges and constraints emerge, many of the considerations discussed in this paper can serve as pathfinder to or directly benefit the architecture and implementation of these missions.

Acknowledgments

The work described in this paper was carried out at the Jet Propulsion Laboratory (JPL), California Institute of Technology, under a contract with NASA. The authors would like to thank Mike Watkins and Frank Webb, the former and current GRACE-FO Project Scientists, and Phil Morton, the GRACE-FO Project Manager; they were instrumental in architecting and executing the GRACE-FO project, respectively. The German Center for Geodesy (GFZ) contributed the launch vehicle, the five year mission operations, and part of the laser ranging interferometer, and the authors would like to acknowledge Frank Flechtner, the GFZ Project Manager. In addition, the authors would like to recognize the many contributions of the entire GRACE-FO Project Office, Project and Flight Systems Engineering teams, the Science and Science Data System teams, the MWI team, and the Mission Assurance and Mission Operations teams. In particular, the authors would like to thank Gerhard Kruizinga of JPL for his support throughout the authoring of this paper. The GRACE-FO spacecraft were built by Airbus Defence and Space under a contract with JPL, and the authors would like to acknowledge the entire Airbus team. The ACC was supplied by ONERA under a contract with JPL. The authors would like to thank Bruno Christophe, the ACC Project Manager, for providing the ACC images, and would like to recognize the entire instrument team. The LRI is an equal partnership between the United States and Germany. The authors acknowledge Gerhard Heinzel from the Albert Einstein Institute as the German Instrument Manager, the German implementation team under the responsibility of SpaceTech GmbH Immenstaad, as well as the entire U.S. implementation team.

References

[1] Tapley, B. D., Chambers, D. P., Bettadpur, S., and Ries, J. C., "Large Scale Ocean Circulation from the GRACE GGM01 Geoid," *Geophysical Research Letters*, Vol. 30, No. 22, 2003, pp. OCE 6 1–4. doi:10.1029/2003GL018622

[2] Tamisiea, M. E., Mitrovica, J. X., and Davis, J. L., "GRACE Gravity Data Constrain Ancient Ice Geometries and Continental Dynamics over Laurentia," *Science*, Vol. 316, No. 5826, May 2007, pp. 881–883. doi:10.1126/science.1137157

[3] Anon., *Satellite Gravity and the Geosphere: Contributions to the Study of the Solid Earth and Its Fluid Envelopes*, National Academies Press, Washington, D.C., 1997. doi:10.17226/5767

[4] O'Keefe, J. A., Eckels, A., and Squires, R. K., "Vanguard Measurements Give Pear-Shaped Component of Earth's Figure," *Science*, Vol. 129, No. 3348, Feb. 1959, pp. 565–566. doi:10.1126/science.129.3348.565

[5] Yionoulis, S. M., "The Transit Satellite Geodesy Program," *Johns Hopkins APL Technical Digest*, Vol. 19, No. 1, 1998, pp. 36–42.

[6] Willis, P., Fagard, H., Ferrage, P., Lemoine, F. G., Noll, C. E., Noomen, R., Otten, M., Ries, J. C., Rothacher, M., Soudarin, L., et al., "The International DORIS Service (IDS): Toward Maturity," Advances in Space Research, Vol. 45, No. 12, 2010, pp. 1408–1420. doi:10.1016/j.asr.2009.11.018

[7] Anon., "Das Schwerefeld der Erde," Geotechnologien, Potsdam, Germany, 2013, http://www.geotechnologien.de/index.php/de/blaue-hefte.html.

[8] Tapley, B. D., Bettadpur, S., Watkins, M., and Reigber, C., "The Gravity Recovery and Climate Experiment: Mission Overview and Early Results," *Geophysical Research Letters*, Vol. 31, No. 9, 2004, Paper L09607. doi:10.1029/2004GL019920

[9] Wolff, M., "Direct Measurement of the Earth's Gravitational Potential Using a Satellite Pair," *Journal of Geophysical Research*, Vol. 74, No. 22, Oct. 1969, pp. 5295–5300. doi:10.1029/JB074i022p05295

[10] Zlotnicki, V., Bettadpur, S., Landerer, F. W., and Watkins, M. M., "Gravity Recovery and Climate Experiment (GRACE): Detection of Ice Mass Loss, Terrestrial Mass Changes, and Ocean Mass Gains," *Earth System Monitoring*, edited by J. Orcutt, Springer Science+Business Media, New York, 2013, p. 123. doi:10.1007/978-1-4614-5684-1_7

[11] Cazenave, A., and Chen, J., "Time-Variable Gravity from Space and Present-Day Mass Redistribution in the Earth System," *Earth and Planetary Science Letters*, Vol. 298, Nos. 3–4, 2010, pp. 263–274. doi:10.1016/j.epsl.2010.07.035

[12] Bettadpur, S., "Orbital Mechanics, Perturbations, and Grace Science and Mission Design," *Advances in the Astronautical Sciences*, Vol. 130, AAS Paper 08-179, 2008.

[13] Park, R. S., Asmar, S. W., Fahnestock, E. G., Konopliv, A. S., Lu, W., and Watkins, M. M., "Gravity Recovery and Interior Laboratory Simulations of Static and Temporal Gravity Field," *Journal of Spacecraft and Rockets*, Vol. 49, No. 2, 2012, pp. 390–400. doi:10.2514/1.A32117

[14] Bergé, J., Christophe, B., and Foulon, B., "GOCE Accelerometers Data Revisited: Stability and Detector Noise," *Proceedings of ESA Living Planet Symposium 2013*, ESA SP-722, Dec. 2013.

[15] Steiger, C., Romanazzo, M., Emanuelli, P. P., Floberghagen, R., and Fehringer, M., "The Deorbiting of ESA's Gravity Mission GOCE—Spacecraft Operations in Extreme Drag Conditions," *SpaceOps 2014 Conference*, AIAA Paper 2014-1934, May 2014. doi:10.2514/6.2014-1934

[16] Dunn, C., Bertiger, W., Bar-Sever, Y., Desai, S., Haines, B., Kuang, D., Franklin, G., Harris, I., Kruizinga, G., Meehan, T., et al., "Instrument of Grace—GPS Augments Gravity Measurements," *GPS World*, Feb. 2003, pp. 16–28.

[17] Christophe, B., Boulanger, D., Foulon, B., Huynh, P.-A., Lebat, V., Liorzou, F., and Perrot, E., "A New Generation of Ultra-Sensitive Electrostatic Accelerometers for GRACE Follow-On and Towards the Next Generation Gravity Mission," *Acta Astronautica*, Vol. 117, Dec. 2015, pp. 1–7. doi:10.1016/j.actaastro.2015.06.021

[18] Flury, J., Bettadpur, S., and Tapley, B., "Precise Accelerometry Onboard the GRACE Gravity Field Satellite Mission," *Advances in Space Research*, Vol. 42, No. 8, 2008, pp. 1414–1423. doi:10.1016/j.asr.2008.05.004

[19] Touboul, P., Foulon, B., Rodrigues, M., and Marque, J. P., "In Orbit Nano-G Measurements, Lessons for Future Space Missions," *Aerospace Science and Technology*, Vol. 8, No. 5, 2004, pp. 431–441. doi:10.1016/j.ast.2004.01.006

[20] Sheard, B. S., Heinzel, G., Danzmann, K., Shaddock, D. A., Klipstein, W. M., and Folkner, W. M., "Intersatellite Laser Ranging Instrument for the GRACE Follow-On Mission," *Journal of Geodesy*, Vol. 86, No. 12, Dec. 2012, pp. 1083–1095. doi:10.1007/s00190-012-0566-3

[21] Abich, K., Bogan, C., Braxmaier, C., Danzmann, K., Dehne, M., Gohlke, M., Görth, A., Heinzel, G., Herding, M., Mahrdt, C., et al., "GRACE Follow-On Laser Ranging Interferometer: German Contribution," *10th International LISA Symposium (LISAX), Journal of Physics*, Conference Series, Vol. 610, 2015, pp. 1–5. doi:10.1088/1742-6596/610/1/012010

[22] Langelüddecke, E., Doll, B., Lampen, M., and Settelmeyer, E., "FLEXBUS—Small Satellites for Science and Earth Observation," *Proceedings of the Euro-Asia Space Week on Cooperation in Space: 'Where East & West Finally Meet*, ESA SP-430, Feb. 1999, pp. 421–427.

[23] Lampen, M., Zaglauer, A., and Settelmeyer, E., "Champ and Grace: FLEXBUS Small Satellites in Orbit," *23rd International Symposium on Space Technology and Science*, Japan Soc. for Aeronautical and Space Science, Matsue, Japan, May–June 2002; also ISTS Paper 2002-f-10, 2002, pp. 1–6.

[24] Gath, P., "Entwicklung, Integration und Test der GRACE Follow-On Satelliten," Document ID: 420305, Deutscher Luft- und Raumfahrtkongress, 2016, www.dglr.de/publikationen/2016/420305.pdf [retrieved 16 Nov. 2017].

[25] Wang, F., Bettadpur, S., Save, H., and Kruizinga, G., "Determination of Center-of-Mass of Gravity Recovery and Climate Experiment Satellites," *Journal of Spacecraft and Rockets*, Vol. 47, No. 2, 2010, pp. 371–379.
doi:10.2514/1.46086

[26] Abich, K., Abramovici, A., Baatzsch, A., Bachman, B., Barr, D., Bize, M., Bogan, C., Braxmaier, C., Burke, M., Clark, K., et al., "Laser Ranging Interferometry with Sub-Nm Noise over 200 km Between the GRACE Follow-On Satellites," *Physical Review Letters* (unpublished).

[27] Schlepp, B., Kirschner, M., Sweetser, T. H., Klipstein, W. M., and Dubovitsky, S., "Flight Dynamics Challenges for the GRACE Follow-On Mission," *25th International Symposium on Space Flight Dynamics*, 2015, pp. 1–16, http://issfd.org/2015/index.php/final-program.html.

J. McMahon
Associate Editor